

AD-A078 483 STANFORD UNIV CA EDWARD L GINZTON LAB  
RESEARCH ON NONDESTRUCTIVE TESTING.(U)  
OCT 79 G S KINO

F/G 14/2

UNCLASSIFIED GL-3049

AFOSR-78-3726

AFOSR-TR-79-1261

NL

| OF |  
AD  
A078483



END  
DATE  
FILED  
1-80  
DDC

ADA078483

19  
48 AFOSR TR- 79-1261

5

FINAL REPORT

6 RESEARCH ON NONDESTRUCTIVE TESTING

LEVEL

for

Air Force Office of Scientific Research

15  
Grant AFOSR-78-3726

for the period

September 1, 1978 - August 31, 1979

9 Final rep. 1 Sep 78-31 Aug 79

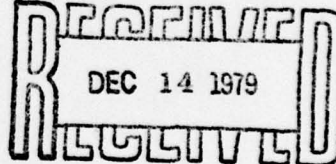
11

OCTOBER 1979

12

51

DDC



G. L. Report No. 3049

10  
Principal Investigator: G. S. Kino

14 GL-3049

Edward L. Ginzton Laboratory/  
W. W. Hansen Laboratories of Physics  
Stanford University  
Stanford, California

Approved for public release;  
distribution unlimited.

Accession For	
NTIS GRAZI	<input checked="" type="checkbox"/>
DDC TAB	<input type="checkbox"/>
Unannounced	<input type="checkbox"/>
Justification	<input type="checkbox"/>
By	
Distribution/	
Availability Codes	
Avail and/or special	
Dist.	

79 12 10 116  
409 640

50B

THIS DOCUMENT IS BEST QUALITY PRACTICABLE.  
THE COPY FURNISHED TO DDC CONTAINED A  
SIGNIFICANT NUMBER OF PAGES WHICH DO NOT  
REPRODUCE LEGIBLY.

## RESEARCH ON NONDESTRUCTIVE TESTING

### I. INTRODUCTION

The aim of this year's work has been to establish new techniques for measuring the properties of materials with the ultimate aim of determining material properties such as hardness and yield strength and being able to predict the life and servicability of mechanical structures. We have limited ourselves to acoustic measurement techniques. Our purpose is to correlate the results of acoustic measurements with the mechanical properties of the material of interest.

The project has been divided into two parts: (1) the characterization of microstructure by acoustic NDE, and (2) the measurement of stress states by acoustic NDE.

The first year's work on characterization of microstructure has been very successful. We have shown that:

1. Relative velocity change measurements can be used to map microstructure with precision in a given piece of steel. We have made the first measurements of hardness variation along a Jominy test bar by acoustic methods. These results are in excellent agreement with the more conventional, much slower technique using a Knoop hardness indentor for determining hardness.
2. We have shown that absolute velocity measurements can be carried out extremely accurately. But they are normally subject to large random variations from sample to sample, due to minor variations of the constituents of the alloys in typical structural steels.

AIR FORCE OFFICE OF SCIENTIFIC RESEARCH (AFSC)  
NOTICE OF TRANSMITTAL TO DDC

This technical report has been reviewed and is approved for public release IAW AFN 190-12 (7b). Distribution is unlimited.

A. D. BLOSE  
Technical Information Officer

3. Acoustic attenuation measurements are very sensitive to micro-structure and have good potential for practical microstructural NDE. We have developed an automatic method for measuring attenuation in materials over a wide frequency range which ultimately should enable us to measure microstructural variations through the depth of a metallic sample. This should have applications to such measurements as those of case hardening.

4. During the course of development of these measurements, we have improved our existing computer controlled velocity measurement system so that it can routinely measure relative velocity to 1 part in  $10^6$  at any point of a flat metal sample.

Our techniques for measuring the stress state of the materials have also made good progress. We have developed a fairly complete theory which shows that it is possible to measure by acoustic methods the so-called J and M energy integrals in the neighborhood of a crack. The evaluation of these integrals makes it possible to determine whether a crack will rapidly grow when a given stress is applied to a structure, a property which is normally very difficult to measure. In related experimental work on another contract, we have carried out experiments which have confirmed some of our initial hypotheses and which show that indeed it is possible to measure these J and M integrals. On this grant, we developed the basic theory required for this purpose.

In addition, we have developed a completely new theory which generalizes these concepts to piezoelectric materials and to thermoelastic effects and magnetoelastic effects. Some unexpected results have been obtained which in fact turned out to have been measured experimentally some time ago in unpublished work. For instance, it was shown that the

presence of an electric field in a piezoelectric material could affect the rate of growth of a crack.

The theories developed are far more general than are required for the evaluation of the single crack. As we have shown, it is also possible to determine whether cracks are present, and to determine the energy associated with a large number of microcracks in a fatigued structure or a welded structure.

Thus, in summary, we are in the process of developing entirely new measurement techniques for metal, ceramic, and other solid structures.

## II. CHARACTERIZATION OF MICROSTRUCTURE BY ACOUSTIC NDE

(J. Shyne, G. S. Kino, D. Ilić, F. Stanke, N. Grayeli)

### A. Introduction

Mechanical properties of materials, such as tensile strength, hardness, and impact toughness, are strongly dependent on microstructural features like grain size and shape, the proportions and spatial distribution of phases present, and macroscale heterogeneities in microstructure resulting from local compositional or thermal-mechanical processing variations. This is true of both metallic and ceramic materials. The microstructural character of materials and their related properties are usually assessed by microscopic examination or by direct measurement of properties; such procedures are often costly and are necessarily destructive, requiring sacrificial example specimens.

We have made considerable progress toward the goal of using acoustic techniques to characterize microstructure in materials nondestructively. The greatest success has been gained by means of acoustic velocity measurements; however, acoustic attenuation measurements are also being used. In the long run, attenuation measurements ought to be more versatile and more useful than velocity measurements. Progress to date with attenuation measurements has mostly been in equipment and technique development.

### B. Measurement Techniques

Significant improvements and new developments have been introduced in our techniques for very precise measurements of velocity and attenuation

of acoustic waves propagating through solid samples. All these measurements are performed using commercial non-bonded transducers, using multiple pulse-echo methods, so that the effects of the liquid buffer are cancelled out from the measurements. The measurements are also interfaced to an on-line computer, which performs data collections, reduction, and correction for extraneous effects (e.g. diffraction, transducer response, buffer/sample reflections), and presentation of two-dimensional velocity fields in the sample, or frequency dependence of the corrected attenuation.

### 1. Velocity Measurement Technique

The electronic signal processing section of our existing set-up was completely rebuilt in order to eliminate problems with long-term drifts which had limited its accuracy in the past. In particular, the receiver chain was completely replaced with a variable-gain amplifier which enables us to measure velocity in samples with wide variation in losses; the detector section was rebuilt to improve the rejection of high-frequency noise; a lock-in amplifier with a tuned signal channel replaced the old combination of a linear gate and tuned amplifier, and an analog phase-lock loop was introduced at the system output. All of these changes have resulted in more than an order of magnitude improvement of the system precision, to the present value of  $10^{-6}$ . This is much smaller than the effects which we are measuring in both our studies of stress and micro-structure, which are of the order of 0.1% or larger.

### 2. Absolute Velocity Measurements

Five specimens of plain carbon steel were prepared by machining 1 cm thick flat plates oriented both longitudinally and transversely relative

to the steel bar stock. Since the acoustic wave propagation direction was through the 1 cm plate thickness, acoustic velocity could be measured both parallel to and transverse to the rolling direction for each steel composition to detect the influence of any preferred orientation or crystal texturing. The compositions of the steels are shown in Table I. All specimens were given identical heat treatment; they were heated to 900°C and air cooled (normalized). This resulted in homogeneous pearlite/ferrite microstructures, the pearlite varying from 12 to 100 volume pct. over the range of carbon contents. After machining, the flat specimens were lapped to assure that their flat surfaces were parallel to within 2.5  $\mu$ m.

The resulting velocity measurements, which include correction for diffraction effects, exhibited random scatter that totally obscured the variation of velocity anticipated from the variation in microstructure. One can easily calculate an expected acoustic velocity from the known densities of pure iron ferrite<sup>2</sup> and Fe<sub>3</sub>C,<sup>3</sup> and known elastic constant data for ferrite/Fe<sub>3</sub>C mixtures.<sup>4</sup> Increasing carbon should cause a decrease in the longitudinal acoustic velocity linearly proportional to carbon content; velocity should decrease 0.85 pct. per wt. pct. carbon in the steel, all other factors being identical. The scatter observed in the measured velocity was not caused by variations in preferred orientation. Had there been any significant degree of preferred orientation, the longitudinal and transverse velocities would differ much more than the slight variations observed. We believe that the random variations in such elements as manganese, silicon, sulfur, and others always present in at least trace amounts, cause variations in density and elastic modulus and thus introduce random variations in acoustic

velocity equal to or greater than the systematic effect of carbon in changing the microstructure. For example, we have calculated that the range of manganese contents in our specimens (see Table I) causes density variations large enough to obscure all the above change attributable to variations in microstructure.

Therefore we conclude that absolute velocity measurements are not practical means for characterizing steel microstructure, because random compositional variations will confuse any attempt to calibrate absolute acoustic velocity variations with microstructure. Similar small compositional differences also occur in nonferrous alloys; this can be expected to render absolute velocity measurements equally impractical for the microstructural characterization for such materials as is the case for steels.

TABLE I  
Composition of Plain Carbon Steels Used For  
Acoustic Velocity Measurements

Steel Type (AISI)	C	Mn	Si	P	S
1010	0.10	0.45	0.03	0.007	0.032
1020	0.20	0.52	0.21	0.009	0.028
1035	0.33	0.72	0.17	0.018	0.025
1060	0.55	0.80	0.19	0.012	0.023
1095	0.93	0.50	0.22	0.009	0.030

### 3. Relative Velocity Measurements

If the material composition is uniform within the object (as is usually the case), variations in acoustic velocity can be unequivocally related to microstructural variations from one location to another. There are many situations where microstructure is not uniform and the pattern of microstructural variation is important, e.g. in an induction hardened steel shaft heat treated to be martensitic on the outer surface but pearlitic in its interior. Jominy end-quench test bars provide another example of steel objects containing microstructural gradients. We successfully used relative velocity measurements to survey quantitatively microstructure of end-quench test bars of several different alloy steel compositions.

The Jominy Test or End-Quench Test is the standard metallurgical quality control procedure for measuring the hardening response of heat treatable steels. The end-quench test specimen is a one-inch diameter round bar, four inches long. The bar is heated to about 800°C. It is then placed in a fixture and cooled by a jet of cold water impinged upon one end. This results in uniaxial heat flow toward the water-quenched end, and reproducible cooling rates that decrease with increasing distance away from the rapidly-cooled quenched end. The fast cooling rate at the quenched end causes the formation of hard, strong martensite; the slower cooled end transforms to softer, weaker pearlite or a pearlite and ferrite mixture, depending on composition. At intermediate locations mixed martensite/pearlite microstructures result from the intermediate cooling rates. The position of the transition from martensite to pearlite is a measure of the hardening response. The usual way of assessing the microstructural gradient along the length of an end-quench bar is to survey

the Rockwell C hardness measured on flats ground along the side of the end quench test bar. This is possible because there is a pronounced hardness gradient caused by the microstructural gradient. Although surveying hardness is a great deal easier and less time consuming than directly observing the microstructure under a microscope, the hardness surveys are tedious because up to 60 individual manual hardness measurements may be required to survey a single test bar.

Figure 1 compares a conventional hardness survey with a longitudinal velocity scan of an end-quench test bar of AISI type 4140, a common, low alloy, heat-treatable steel. The acoustic path was transverse to the axis of the test bar. Parallel flats were ground on opposite sides the full length of the test bar; the acoustic path was thus along bar diameters through the thickness of the bar between the ground flats. The relative acoustic velocity is plotted as  $\Delta v/v_0$ , the fractional change in velocity at any point relative to  $v_0$ , the velocity at the slower cooled pearlitic end of the test bar. As seen in the plot, the velocity decreased by about 0.7% at the martensitic, quenched end. The accuracy of the relative acoustic velocity measurement is limited by the uniformity of the thickness and the deviation from perfect parallelism of the ground flats. This is estimated to be 1 or 2 parts in  $10^4$  which is about 2% of the actual range of velocities measured. Thus the sensitivity and discrimination of the velocity measurement is equal to or better than that of the hardness measurements.

The computer controlled automatic acoustic velocity scan requires only 4 minutes from start to finish with the data automatically plotted as  $\Delta v/v_0$  versus position in the bar. This contrasts favorably with the hour or so required for a manual hardness survey. To our knowledge, this

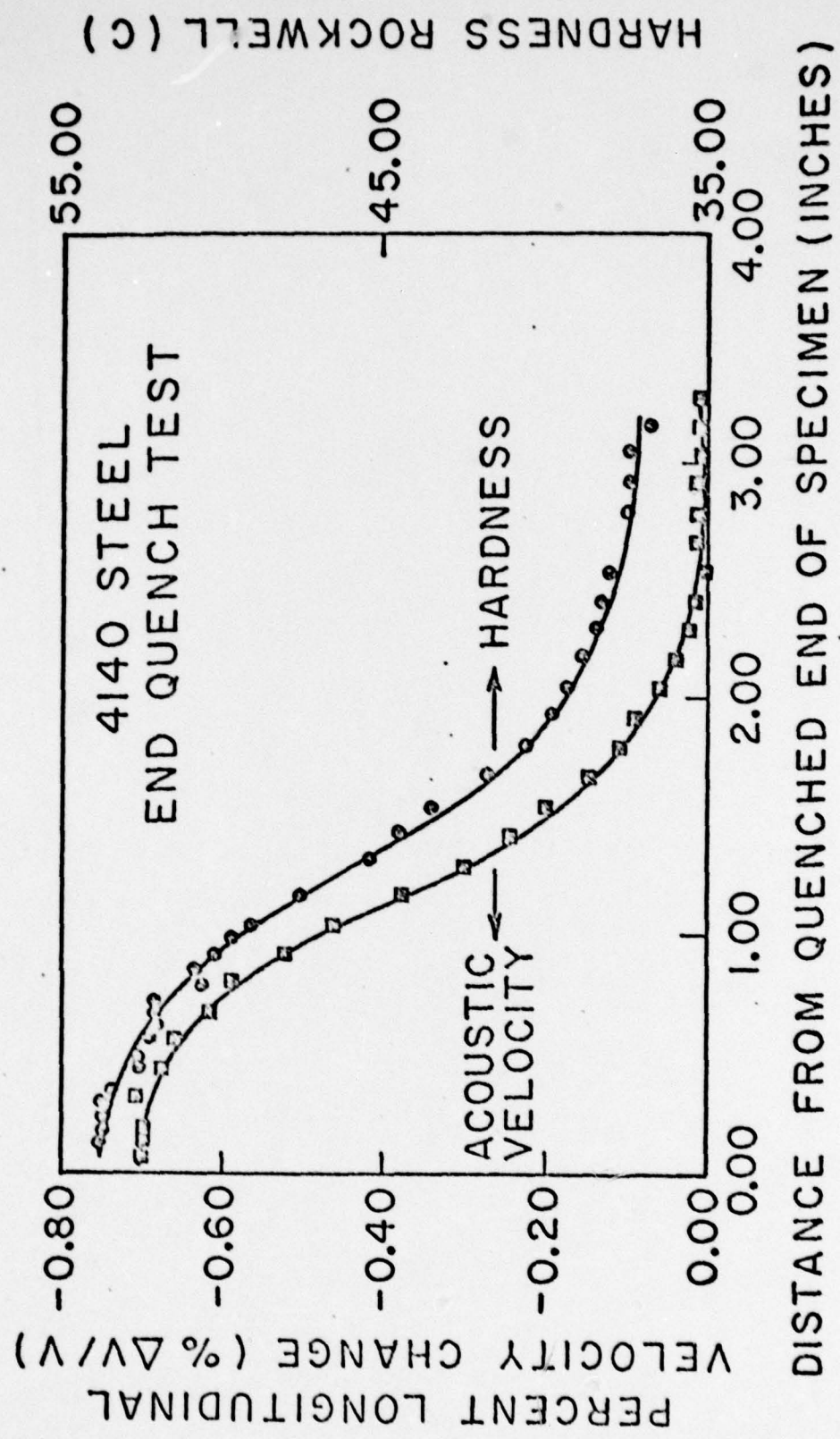


FIG. 1--End-quench test results measured in type 4140 steel. The two curves compare the micro-structure gradient as surveyed acoustically and by conventional hardness measurements.

is the first time an end-quench test has been performed using a velocity scan rather than a hardness scan.

In addition to the 4140 steel end-quench test, we have also performed similar acoustic velocity scans on end-quench test bars of types 52100, 4615, 8640, and 1095 steels with similarly encouraging results. We find these results persuasive that acoustic velocity measurements can be used to map out microstructural variations within steel objects.

### C. Acoustic Attenuation Measurements

In principle, attenuation measurements are more attractive than velocity measurements as the basis of acoustic NDE microstructural characterization. Where velocity is weakly a function of microstructure, acoustic attenuation is strongly affected by microstructure because of scattering at grain boundaries, second phase particles, and other microstructural features. Moreover, the strong frequency dependence of the acoustic attenuation coefficient can provide additional information related to microstructure.

A sophisticated technique has been developed for automatically measuring, calculating, and displaying the attenuation of acoustic waves through solid samples for a wide range of frequencies. The technique consists of launching a broadband pulse of acoustic wave energy into the sample through a buffer and then recording the echoes from the front face, as well as the first, and the second back-face echo from the sample. The three pulses are then digitized and stored in computer memory, and subsequently used as the basis for introducing corrections due to transducer response, reflections from buffer/sample interfaces, and for calculating the attenuation of the material. The individual

frequency components of the broadband pulses are corrected in amplitude for diffraction effects, and the attenuation as a function of frequency is plotted direction by the computer. Signal averaging and/or sampling techniques are also used for increasing the signal-to-noise ratio, and for processing signals in the frequency range from 5 to 70 MHz.

Figure 2 shows the attenuation in two different steel samples with identical compositions but different microstructure. The curves for pearlite and martensite show frequency dependences close to  $f^4$  indicating that Rayleigh scattering is the dominant mechanism for attenuation. Pearlitic data was obtained from two different transducers as shown by the overlap on the figure. These first results demonstrate the ability of our attenuation measuring technique to discriminate between steel microstructures. A variety of experiments are in progress to apply the method to steels, copper, and aluminum alloys. We believe that attenuation measurements can be used to gain much useful information about the microstructural state of materials.

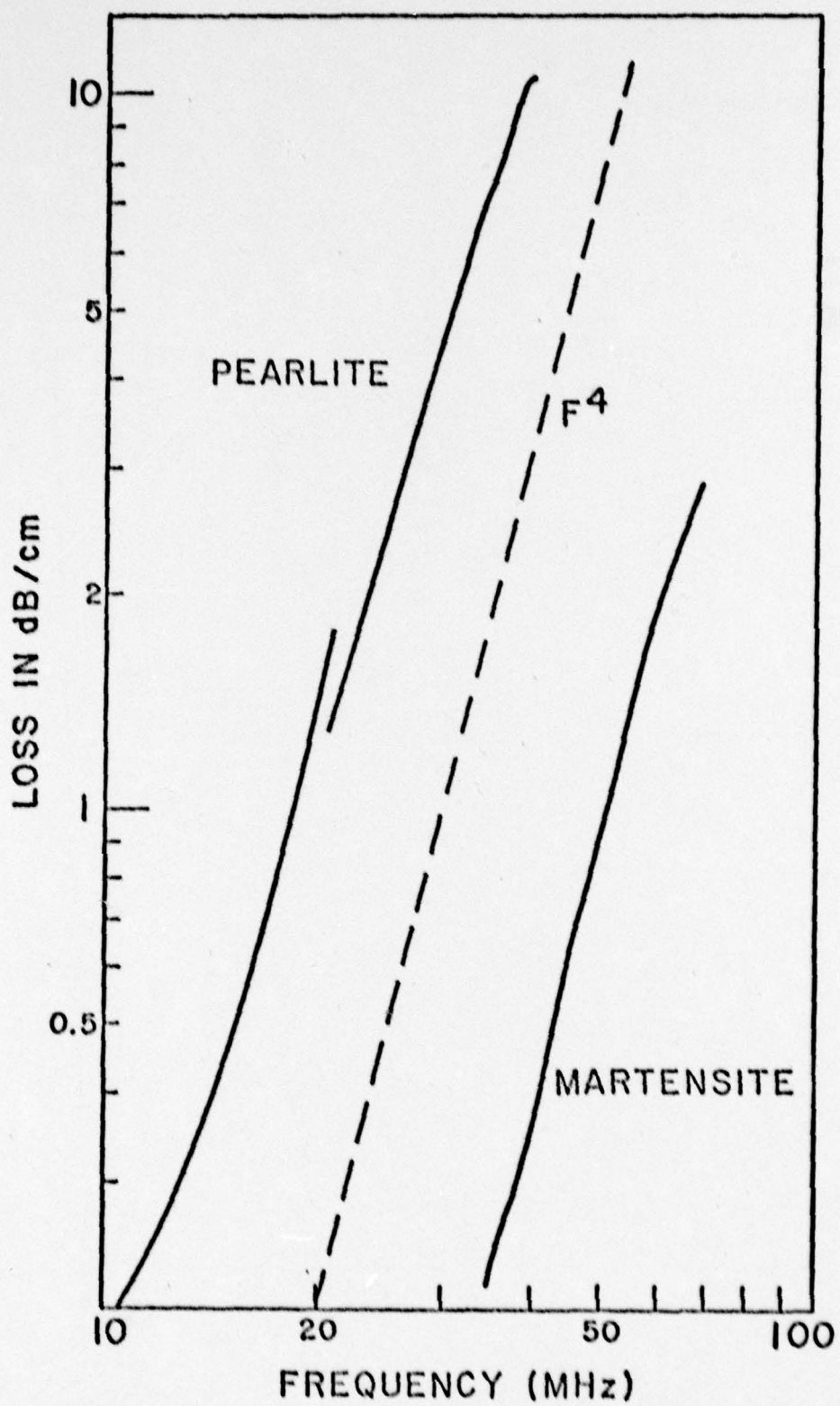


FIG. 2--Attenuation versus frequency for two specimens of the same steel heat treated differently to have martensite in one but pearlite in the other.

### III. MEASUREMENTS OF STRESS STATES BY ACOUSTIC NDE

(D. Barnett, G. Herrmann, W. F. J. Deeg, and R. King)

#### A. Introduction

In numerous aeronautical and aerospace structural systems it is imperative to have available accurate, reliable methods for periodic nondestructive evaluation of critical parts in order to predict useful service lifetimes. These nondestructive inspections are needed to ensure the integrity of structural elements under complex loading, thermal, and environmental conditions, with particular emphasis on the prevention of catastrophic or brittle failure.

During the past year, we have worked toward developing entirely new techniques for quantitatively determining the states of stress associated with cracks and other sources of stress concentration using acoustic nondestructive methods. In particular, we have made very good progress in developing methods for:

1. Determining whether or not stress concentrations such as flaws, inclusions, or cracks are present; and
2. Assessing whether or not, for given loading conditions, catastrophic failure due to unstable crack propagation is a distinct possibility, without the need for making direct measurements on the stress concentration sites.

At the same time we have recognized that under many technological applications of engineering importance, real materials are often subjected to the effects of rather complex coupled fields, e.g., piezoelectric, magnetoelastic, and thermoelastic fields. The governing fracture mechanics

for materials experiencing coupled fields had not previously been developed, and we have attempted, with success, to construct the extended fracture mechanics framework required. We view this as a significant advance, since, just as in the case of purely elastic solids, the fracture mechanics framework provides the vehicle for successful coupling of theory and experiment.

#### B. The Acoustic Determination of the J and M Integrals in Cracked Plates

Let us consider an elastic solid in a state of two-dimensional plane deformation. The line integrals

$$J = \oint_c (W dy - T_i \frac{\partial u_i}{\partial x} ds) \quad (1)$$

$$M = \oint_c (W n_i x_i - T_K \frac{\partial u_K}{\partial x_i} x_i) ds \quad (2)$$

may be shown to yield the generalized thermodynamic forces (so-called crack extension forces) on single-ended and double-ended sites of stress concentrations with the contour  $c$ . Here  $W$  is strain energy density,  $\vec{T}$  and  $\vec{u}$  are the traction and displacement vectors, respectively,  $\vec{n}$  is the outer normal to  $c$ , and  $ds$  and  $dy$  are, respectively, an element of arc of  $c$  at  $\vec{x}$  and its component along the  $y$ -direction.

If  $c$  contains one tip of a crack parallel to the  $x$ -direction, then

$$J = \frac{1 - \nu^2}{E} (K_I^2 + K_{II}^2) \equiv G \quad (3)$$

where  $\nu$  and  $E$  are Poisson's ratio and Young's modulus, respectively,

$K_I$  and  $K_{II}$  are the Mode I and Mode II crack stress intensity factors, and  $G$  is the crack extension forces. Similarly, one can show that if  $c$  encloses both tips of a crack of length  $\ell$  then

$$M \equiv \ell G . \quad (4)$$

Both  $J$  and  $M$  are path-independent so that the contour  $c$  is quite arbitrary and may be chosen for both theoretical and experimental convenience. Since the usual fracture criterion is expressed as

$$G = G_c \quad (5)$$

where  $G_c$  is the fracture toughness which is a material property and determinable by separate destructive measurements; it is immediately clear that if one can determine  $J$  and  $M$  nondestructively, say, by acoustic methods, one can use this information to:

1. Determine whether or not stress concentration sites exist in a given region, i.e., if both  $J$  and  $M$  vanish there are no such sites; and
2. If stress concentration sites exist, determine whether or not  $G$  is dangerously close to  $G_c$ .

During the past year we have shown that it is indeed possible and practical to determine  $J$  and  $M$  from acoustic measurements on loaded cracked panels from measurements of the relative velocity shift of longitudinal and shear waves propagating through the panels. It is known that longitudinal and shear wave scans of stressed samples allow one to determine the in-plane principal stresses  $\sigma_1$  and  $\sigma_2$  as well as the orientation  $\theta$  of the principal stress axes at selected points in such samples. During the past year we performed an analysis (R. King, G. Kino,

and D. Barnett, in preparation) which shows that  $J$  may be expressed as

$$J = -\frac{1-v^2}{2E} \int \phi (\sigma_1 - \sigma_2)(\sigma_1 + \sigma_2) \cos(2\theta - \phi) ds - \frac{1}{2} \int \phi \omega \{(\sigma_1 - \sigma_2) \sin(2\phi - \theta) + (\sigma_1 + \sigma_2) \sin \theta\} ds . \quad (6)$$

All quantities in the integrands in (6) are determinable directly from acoustic data except for the rotation field  $\omega$ , which can be found from forward integration of the compatibility equations expressed in terms of the acoustically measured stress state. A result similar to (6) holds for the  $M$  integral. Thus, in principle, both  $J$  and  $M$  may be found from nondestructive acoustic measurements alone.

For the past two years we have had and are refining a scanning longitudinal wave system capable of performing the requisite acoustic measurements; development of a scanning shear wave system is now well underway. During the past year we have demonstrated by computer simulation using exact elastic fields with superimposed random noise to simulate experimental error to show that acoustic determination of  $J$  and  $M$  is indeed feasible.

It has also been clear that a successful program to acoustically determine  $J$  and  $M$  must involve comparison with theory. To this end, one requires theoretical knowledge of the exact elastic fields at points in geometrically complex plane laboratory samples under external loading. Such complete solutions are almost never available in the literature. During the past year we have developed a Boundary Integral Equation computer code capable of solving problems of cracked elastic plates of arbitrary geometry and of arbitrary elastic anisotropy. The technique

will not be described here, but we note that development of such codes has been supported in other laboratories by other branches of AFOSR. To our knowledge, ours is the first Boundary Integral Code valid for arbitrary anisotropy. The computer program is quite compact and user-oriented. A paper describing the program (D. Barnett and R. King) is currently being prepared.

### C. Stress Analysis and Fracture Mechanics in Solids Containing Cracks and Inclusions and Subjected to Coupled Fields

We have generated the first complete solution for the stress analysis and fracture mechanics of a slit-like crack in a piezoelectric solid of arbitrary anisotropy (piezoelectrics are necessary anisotropy). This work is currently being prepared for publication (W. F. J. Deeg and D. Barnett, to be submitted to International Journal of Solids and Structures). The stress analysis developed shows how both externally applied loads and electric fields influence the stress intensity factors and the crack extension force in such media. A remarkable result of the analysis is that the crack extension force may be either positive, negative, or zero depending upon the ratio of applied tractions to the applied electric field! In essence, this means that given a cracked piezoelectric with certain applied loadings, the crack may be rendered either stable or unstable by varying the applied electric field appropriately. The extension of the J and M integrals to such solids has also been made.

An analysis with even more far-reaching consequences has been developed for problems of piezoelectrics containing voids and inhomogeneities has been completed (W. F. J. Deeg and D. Barnett, to be submitted to International Journal of Engineering Science). We have extended a previous

analysis by J. D. Eshelby for "transformed" elastic inclusions and inhomogeneities to the piezoelectric case. These are fully three-dimensional anisotropic solutions. The problems concerned the fields associated with inclusions and inhomogeneities which, in the absence of a surrounding matrix, would like to take on a stress-free or "transformation" strain. The constraint of the surroundings induces an initial stress and strain state in the entire medium. The transformation strain may arise from a phase transformation or be due to thermal mismatch; a slight re-interpretation of the transformation strain allows us to completely treat the problem of stress concentrations about ellipsoidal voids and inclusions perturbing far-field applied loadings and electric fields in a very simple way. Hence, we now feel that we have made a rather complete development for treating problems of stress concentrations in infinite piezoelectric solids.

For piezoelectric solids of finite dimensions and complex boundary shapes we have formulated the appropriate Boundary Integral Equation method for generating the solutions of interest to us. This involves a minor overhaul of our previously-mentioned Boundary Integral Code for pure elastic solids, and we anticipate that the computational scheme will be fully operational within the coming year.

Finally, we note that the notion of conservation integrals, the  $J$  and  $M$  integrals, for thermoelastic and porous solids has been treated during the last year.

## REFERENCES

1. D. B. Ilić, G. S. Kino, A. R. Selfridge, and F. E. Stanke, "Computer-Controlled System for Measuring Two-Dimensional Acoustic Velocity Fields," presented at the IEEE Ultrasonics Symposium, New Orleans, Louisiana, September 1979.
2. D. B. Ilić, G. S. Kino, and A. R. Selfridge, "Computer-Controlled System for Measuring Two-Dimensional Acoustic Velocity Fields," to be published in Rev. Sci. Instrum., December 1979.
3. N. Grayeli, D. B. Ilić, F. Stanke, G. S. Kino, and J. C. Shyne, "Acoustic Measurement of Microstructures in Steels," presented at the ARPA/AFML Review of Progress in Quantitative NDE, La Jolla, California, July 1979.
4. D. Barnett, G. Herrmann, J. Hunter, R. King, D. Ilić, and G. S. Kino, "The Use of Acoustoelastic Measurements to Characterize the Stress States in Cracked Solids," presented at the ARPA/AFML Review of Progress in Quantitative NDE, La Jolla, California, July 1979.
5. N. Grayeli, F. Stanke, C. H. Chou, D. B. Ilić, and J. C. Shyne, "Studies of Steel Microstructures by Acoustical Methods," presented at the IEEE Ultrasonics Symposium, New Orleans, Louisiana, September 1979.
6. G. Herrmann, "Some Applications of Invariant Variational Principles in Mechanics of Solids," presented at the IUTAM Symposium on Variational Methods in the Mechanics of Solids, Evanston, Illinois, September 1978.

**APPENDIX**

SOME APPLICATIONS OF INVARIANT VARIATIONAL  
PRINCIPLES IN MECHANICS OF SOLIDS

by

George Herrmann  
Division of Applied Mechanics  
Stanford University  
Stanford, California

Abstract

Based on invariant variational principles due to Noether, it is possible to derive several conservation theorems of mathematical physics applicable, in principle, for any field theory. These conservation laws, and the resulting so-called path-independent integrals, have proved useful in continuum mechanics and in particular in the theory of elasticity.

Several new applications of these conservation theorems will be discussed, including specifically those to elastodynamics, thermoelasticity, porous media, and the experimental determination of stress intensity factors in fracture mechanics.

## 1. INTRODUCTION

A celebrated theorem due to Emmy Noether (1882-1935) [1] makes it possible to construct divergence-free quantities from the variables of a variational problem, provided the extremum integral possesses certain invariance properties.

If Hamilton's Principle is applied to derive variationally the equations of motion of a physical theory, one obtains merely the Euler-Lagrange equations because the domain ("fixed endpoint variation") itself is not varied.

By contrast, if the same variational integral (whose integrand is the Lagrangian density) is subjected to a more general type of variation, allowing endpoint variations, certain additional terms do appear, along with the terms corresponding to the Euler-Lagrange equations.

The additional terms form a tensor, referred to as the energy-momentum tensor. Its usefulness in continuum mechanics, and particularly in the theory of elasticity, as discussed by Eshelby in a series of papers beginning in 1951 [2, 3, 4], rests on the fact that the energy-momentum tensor leads to conservation integrals (so-called "path-independent" integrals) which have an immediate physical significance. Limited availability of space does not permit here a detailed discussion of these integrals. It will suffice to mention that the so-called translation integral, first discussed by Eshelby [2], represents a force on a defect. A defect is defined in this context as any type of nonhomogeneity, inclusion, cavity, dislocation, crack, etc. The "force" on a defect is not the customary Newtonian force, but is defined, rather, as the rate of change of total energy of the system with respect to a unit infinitesimal displacement of the defect.

Quite independently of Eshelby, three conservation laws of elastostatics were derived by Günther [5]. He showed how all three of them could be applied

in problems of torsion, plane stress, beam theory, plate theory, and shell theory. Günther was not interested in defects, but simply in providing expressions of boundary integrals which were path-independent. It can be rigorously shown that in Euclidean space there will be just three conservation laws, because only three groups of infinitesimal transformations satisfy Noether's invariance principle. The three conservation laws are associated with the transformation of translation, rotation and similarity (or gauge), respectively. The translation integral, which provides Eshelby's force on a defect, was independently deduced by Rice [6] for the special case of a crack, which he called the J-integral. The rotation and similarity integrals were independently discovered by Knowles and Sternberg [7], who did not discuss their potential application, but extended them to nonlinear elasticity.

In the context of fracture mechanics, the importance of path-independent integrals resides in the fact that they can be related to energy release rates, i.e. to crack extension forces which themselves depend only on stress intensity factors.

It was shown by Rice [6] that the J-integral is related to the total potential energy-release rate associated with moving or extending cracks (in their own plane) in linear or nonlinear elastic materials. Later, Budiansky and Rice [8] have shown that the two additional integrals of Günther and of Knowles and Sternberg are associated with cavity or crack rotation (they called it the L-integral) and expansion (or similarity, they called it the M-integral), respectively.

In what follows, the energy-momentum tensor is briefly derived and applied to: a) free motions of an elastic bar; b) equilibrium of a thermoelastic solid or fluid-filled porous solid and c) to the experimental determination of stress-intensity factors, making use of the J-integral.

## 2. ENERGY-MOMENTUM TENSOR

As suggested by Eshelby [3,4] and by Kaul [9], the energy-momentum tensor can be derived in a concise fashion without explicit recourse to the calculus of variations. Let the Lagrangian density  $L$  depend on  $n$  independent variables  $x^\alpha$ , on  $m$  dependent functions  $\phi^i(x^\alpha)$ , as well as on the gradients  $\partial\phi^i/\partial x^\alpha \equiv \partial_\alpha \phi^i$ . The Lagrangian density can also be considered a function of only the independent variables, which will be denoted by  $\tilde{L}$ . Thus we can write

$$L = L(x^\alpha, \phi^i, \partial_\alpha \phi^i) = \tilde{L}(x^\alpha) \quad \alpha = 1, 2, \dots, n; i = 1, 2, \dots, m \quad (2.1)$$

If we define

$$\partial L / \partial \phi^i \equiv T_i \quad ; \quad \partial L / \partial \partial_\alpha \phi^i \equiv T_i^\alpha \quad (2.2); (2.3)$$

then the chain rule will give

$$\partial_\alpha \tilde{L} = \partial_\alpha L + T_i \partial_\alpha \phi^i + T_i^\beta \partial_\alpha \partial_\beta \phi^i \quad (2.4)$$

which can also be written as

$$\partial_\alpha \tilde{L} = \partial_\alpha L + T_i \partial_\alpha \phi^i + \partial_\beta (T_\alpha^\beta \partial_\alpha \phi^i) - (\partial_\beta T_i^\beta) \partial_\alpha \phi^i \quad (2.5)$$

or

$$\partial_\alpha \tilde{L} = \partial_\alpha L + (T_i - \partial_\beta T_i^\beta) \partial_\alpha \phi^i + \partial_\beta (T_i^\beta \partial_\alpha \phi^i) \quad (2.6)$$

The parenthesis  $T_i - \partial_\beta T_i^\beta$  is recognized to be the  $i$ -th Lagrange equation of motion which will be abbreviated, as usual by  $[L]_i$ . If the last term in eqn.(2.6) is brought to the left-hand side, this equation may be rewritten as

$$\partial_\beta (\tilde{L} \delta_\alpha^\beta - T_i^\beta \partial_\alpha \phi^i) = \partial_\alpha L + [L]_i \partial_\alpha \phi^i \quad (2.7)$$

The negative of the quantity in parenthesis is defined as the energy-momentum tensor  $P_\alpha^\beta$

$$P_\alpha^\beta \equiv -\tilde{L} \delta_\alpha^\beta + T_i^\beta \partial_\alpha \phi^i \quad (2.8)$$

If all the independent variables are cyclic (or ignorable), i.e.  $\partial_\alpha L = 0$ , and if the equations of motion are satisfied, i.e.  $[L]_i = 0$ , then we see that

$$\partial_\beta P_\alpha^\beta = 0 \quad (2.9)$$

i.e. the energy-momentum tensor is divergence-free. This implies the existence of a potential

$$P_\alpha^\beta = e_\alpha^\gamma e_\sigma^\mu \partial_\gamma \phi^\mu \partial_\sigma^\beta \quad (2.10)$$

It may be remarked further that the energy-momentum tensor is the Hamiltonian of classical dynamics, where one is concerned with only one independent variable (time). Similarly as in classical dynamics, one can derive in the present case of  $n$  independent variables the canonic equations which has been done by Kane [10].

### 3. ELASTIC BAR

As a simple, but not trivial example, let us consider a continuum which would involve two independent variables (and thus be essentially different from classical dynamics) and only one dependent variable. One-dimensional motions in an elastic homogeneous bar represent such a system. The Lagrangian density in usual notation is given by

$$2L = \rho \dot{u}^2 - Eu^2 \quad (3.1)$$

Here  $\rho$  is the mass density per unit of length of the bar,  $E$  is Young's

modulus of the material,  $u$  is the displacement. Dot and prime indicate partial differentiation with respect to time and the  $x$ -coordinate along the bar, respectively.

In terms of the notations introduced in the previous section, we can write

$$i = 1; \alpha = 1, 2; x^1 = x; x^2 = t; u = \phi^1; u' = \partial_1 \phi^1; \dot{u} = \partial_2 \phi^2$$

The components of the energy-momentum tensor in this example are calculated to be

$$P_1^1 = \sigma u'/2 + p \dot{u}/2, P_1^2 = -p u', P_2^1 = \sigma \dot{u}, P_2^2 = -\sigma u'/2 - p \dot{u}/2 \quad (3.2)$$

where  $\sigma$  is the stress and  $p$  the momentum

$$\sigma = E u'; p = \rho \dot{u} \quad (3.3)$$

Since  $L$  does not depend on  $x$  and  $t$  explicitly, and if the equation of motion is satisfied, the energy-momentum tensor is divergence-free which leads in this example to the two Noether equations, in usual notation

$$\partial_x (\sigma u'/2 + p \dot{u}/2) - \partial_t (p u') = 0 \quad (3.4)$$

$$\partial_x (\sigma \dot{u}) - \partial_t (\sigma u'/2 + p \dot{u}/2) = 0 \quad (3.5)$$

It is tempting to try to provide a physical interpretation to the above two equations. The second equation is more familiar in this regard. The product  $\sigma \dot{u}$  is recognized to represent the energy flux across a cross-section of the bar. Since the sum  $\sigma u'/2 + p \dot{u}/2$  represents the total energy density of the bar, the second equation states that the time-rate of change of the total energy of a bar element has to equal the net energy flux within the element. Thus equation (3.5) is a statement of the principle of energy conservation.

To assign a physical meaning to equation (3.4) is not so straight-forward.

If it is recalled that the force on a defect is defined as the spatial rate of change of the total energy, the first term can be looked upon as a kind of force, which could be termed non-Newtonian or quasi-force. The second term has been referred to in the past [3] as quasi-momentum, pseudomomentum, or field momentum. Thus equation (3.4) appears to be a statement of the principle of linear momentum, however not in the ordinary, Newtonian sense, but rather pertaining to the motion of defects with respect to the body. For a further discussion see Eshelby [3,4] and Rogula [11].

In symbolic notation equations (3.4) and (3.5) can be written compactly as

$$\nabla \cdot \mathbf{IP} = 0 \text{ where } \nabla \equiv \frac{\partial}{\partial x} \mathbf{i}_x + \frac{\partial}{\partial t} \mathbf{i}_t \quad (3.6); (3.7)$$

and  $\mathbf{IP}$  is the energy-momentum dyadic with components given in equation (12).

The divergence theorem leads from equation (3.6) immediately to equation

$$\oint \mathbf{n} \cdot \mathbf{IP} ds = 0 \quad (3.8)$$

where  $ds$  is the element of length of any closed circuit in the  $x, t$  plane and  $\mathbf{n}$  is the outward drawn normal unit vector. As a simple application of the path-independent integral (3.8) let us consider a bar of length  $\ell$  and a rectangular circuit as indicated in the sketch, where  $t^*$  is some arbitrary time. Equation (3.8) leads then to the relation

$$\int_0^\ell \sigma u dx \Big|_{t=t^*} = \int_0^\ell \sigma u dx \Big|_{t=0} - \int_0^{t^*} \int_{x=\ell} p u' dt dx - \int_0^{t^*} \int_{x=0} p u' dt dx \quad (3.9)$$

The first term on the right-hand side of equation (3.9) can be evaluated on the basis of prescribed initial conditions. Similarly, the second and third term on the right-hand side can be evaluated on the basis of prescribed boundary conditions. Relation (3.9) may be readily interpreted as stating that the total (in space) energy flux (or power) is conserved in time.

#### 4. THERMOELASTIC SOLID OR FLUID-FILLED POROUS SOLID

Variational principles in thermoelasticity and heat conduction were discussed by Herrmann in [12]. Using the analogy established by Biot [13], the following development is valid also for an elastic porous solid, whose pores are filled with a compressible viscous fluid.

The equilibrium equations can be written down, in the absence of body forces as

$$\tau_{ij,j} - \beta_{ij}\theta_{,j} = 0 \quad ; \quad \theta_{,i} - g_i = 0 \quad (4.1); (4.2)$$

and the constitutive equations as

$$\gamma_{ij} - w_{,ij} = 0 \quad ; \quad \gamma + w_{,\theta} = 0 \quad ; \quad s_i + d_{,g_i} = 0 \quad (4.3); (4.4); (4.5)$$

In these equations  $\tau_{ij} - \beta_{ij}\theta \equiv \sigma_{ij}$  denotes the total stress,  $\tau_{ij}$  is the isothermal part of stress,  $\beta_{ij}$  is related to the thermal expansion properties of the material,  $\theta$  is the temperature increment above a reference absolute temperature  $T_r$ ,  $g_i$  is the thermal disequilibrium force,  $\gamma_{ij} = (u_{i,j} + u_{j,i})/2$  is the elastic strain,  $\gamma = s_{i,i} + \beta_{ij}u_{i,j}$  is the "thermoelastic dilatation". The entropy displacement  $s_i$  is related to the entropy  $s$  by the equation

$$s = -s_{i,i} \quad (4.6)$$

$W$  is Biot's thermoelastic potential, expressed here as a quadratic form of isothermal components of stress and the temperature increment

$$2W = B_{ijkl}\tau_{ij}\tau_{kl} + c\theta^2/T_r \quad (4.7)$$

where  $c$  is the specific heat per unit volume for zero strain.  $D$  is Biot's

dissipation function, expressed here as a quadratic form of the "thermal disequilibrium force"  $g_i$ , the quantity conjugate to the entropy displacement  $s_i$

$$D = k_{ij} g_i g_j / p T_r \quad (4.8)$$

Here  $k_{ij}$  is the thermal conductivity tensor and  $p$  is the time operator  $\partial/\partial t$ . To derive a variational principle for displacements, the constitutive equations are written in inverted form

$$\tau'_{ij} = U_{,ij} \quad ; \quad \theta = -U_{,\gamma} \quad ; \quad g_i = G_{,s_i} \quad (4.9); (4.10); (4.11)$$

where the quadratic forms  $U$  and  $G$  are

$$U = \frac{1}{2} c_{ijkl} \gamma_{ij} \gamma_{kl} + \frac{1}{2} T_r \gamma^2 / c \quad (4.12)$$

$$G = \frac{1}{2} \frac{p T_r}{k_{ij}} s_i s_j \quad (4.13)$$

Consider now the Lagrangian density  $L$  to be  $U - G$  and let the independent variables be  $\gamma_{ij}$ ,  $\gamma$  and  $s_i$ , i.e.

$$L = U - G = L(\gamma_{ij}, \gamma, s_i) \quad (4.14)$$

The thermoelastic energy momentum tensor can then be calculated and can be represented in either one of the following forms

$$P_{ij} = (U - G + \theta\gamma) \delta_{ij} - \tau_{kj} u_{k,i} \quad (4.15)$$

$$P_{ij} = \left( \frac{1}{2} \tau_{kl} \gamma_{kl} + \frac{1}{2} \gamma \theta + \frac{1}{2} s_k g_k \right) \delta_{ij} - \tau_{kj} u_{k,i} \quad (4.16)$$

$$P_{ij} = (U - G - \theta s) \delta_{ij} - \sigma_{kj} u_{k,i} \quad (4.17)$$

$$\text{where } \sigma_{kj} = \tau_{kj} - \beta_{kj} \theta \quad (4.18)$$

Since the energy-momentum tensor is divergence-free, a "path-independent" integral can immediately be constructed formally. In the absence of thermal effects it will reduce to Rice's J-integral. We obtain either one of the following forms

$$J_k = \int [(U - G - \theta s) n_k - n_i \sigma_{ij} u_{j,k}] da \quad (4.19)$$

$$J_k = \int [\frac{1}{2}(\tau_{ij}\gamma_{ij} + \gamma\theta + s_i g_i) n_k - n_i \sigma_{ij} u_{j,k}] da \quad (4.20)$$

$$J_k = \int [\frac{1}{2}(\sigma_{ij}\gamma_{ij} - s\theta + s_i g_i) n_k - T_j u_{j,k}] da \quad (4.21)$$

Integration is to be carried out over a closed surface with element da.

Wherever the time operator  $p \equiv \frac{\partial}{\partial t}$  occurs, the multiplication has to be carried out as convolution, similarly as in the dynamic case discussed by Gurtin [14].

## 5. EXPERIMENTAL DETERMINATION OF STRESS-INTENSITY FACTORS

In some recent and still ongoing experimental studies, the stress-intensity factor at the root of an edge-notched 6061-T6 aluminum specimen in tension has been determined by direct measurement of the J-integral, defined in two dimensions as

$$J = \int_{\Gamma} (W dy - T_i \frac{\partial u_i}{\partial x} ds) \quad (5.1)$$

Here  $\Gamma$  is a curve surrounding the crack tip,  $W$  the energy density,  $x$  and  $y$  are rectangular coordinates parallel and normal to the crack, and  $ds$  is an element of arc length along  $\Gamma$ ,  $T_i$  is the traction vector defined with respect to the outward normal along  $\Gamma$ ,  $u_i$  is the displacement vector.

The value of  $J$  has been determined experimentally by measuring  $W$ ,  $T_i$  and  $\partial u_i / \partial x$  on the rectangular contour of the test specimen. The specimen

was 1.0 cm thick, 6.0 cm wide and the distance between shoulders was 15.2 cm. The edge crack was placed midway between shoulders and had a depth of 0.96 cm. If the specimen is thought to be in vertical position, then along the vertical edges  $T_i = 0$  and the contribution to  $J$  is only from  $\int W dy$ . Across the top and bottom of the sample  $dy = 0$  and  $ds = dx$  such that only  $-\int T_i (\partial u_i / \partial x) dx$  contributes to  $J$ . To evaluate  $W$ , 10 strain gages were placed along the upper half only (due to symmetry) of the vertical edges and it was assumed that the specimen was linearly elastic everywhere, thus  $W = E\epsilon^2/2$  where  $E$  is Young's modulus and  $\epsilon$  is the strain. Further,  $W$  is proportional to  $P$ , the load on the sample. The dimensions of the specimen were chosen such that the strain just below the shoulders of the tension specimen would be approximately uniform. This  $\partial u_i / \partial x$  could be determined with good accuracy using only several points across the specimen, obtaining nearly the same value (rigid rotation).

The contribution to  $J$  from the vertical edges (strain gage measurements) was determined to be

$$J_V = 0.252 \times 10^{-17} P^2 E \frac{m}{N^2} \quad (5.2)$$

The contribution to  $J$  from the horizontal portion of the contour, measured by means of linear variable differential transformers (LVDT) as displacement gages was found to be

$$J_H = 1.96 \times 10^{-17} P^2 E \frac{m}{N^2} \quad (5.3)$$

Addition gives the total contribution to  $J$

$$J = J_V + J_H = 2.21 \times 10^{-17} P^2 E \frac{m}{N^2} \quad (5.4)$$

The equivalent stress intensity value is  $K = [JE/(1 - v^2)]^{1/2}$  for plane strain cracks. Thus the experimental method permitted to measure  $K/E$ . This can be compared with the calculated handbook value [15], which is

$$J = 2.15 \times 10^{-17} P^2 e^{-\frac{m}{N^2}}$$

Here a value of  $E = 7.03 \times 10^{10} \text{ N/m}^2$  has been used.

It is seen that the agreement between the theoretical and the measured value of  $J$  is excellent. Note that only about 10% of the value of  $J$  stems from the vertical part of the integral for the specimen with the described geometry. A more detailed account of this investigation is given in ref. [16].

#### ACKNOWLEDGMENT

The work summarized in this paper was supported, in part, by EPRI Contract No. RP-609-1, by NSF Contract No. DMK-76-00726 through the Center for Materials Research at Stanford University, and by AFOSR Grant 78-3726.

#### REFERENCES

1. Noether, E., "Invariante Variationsprobleme, Göttinger Nachrichten, Mathematisch-physikalische Klasse, Vol. 2 (1918) 235. English translation in Transport Theory and Statistical Physics, Vol. 1 (3) (1971) 183-207.
2. Eshelby, J.D., "The Force on an Elastic Singularity," Phil Trans. Roy. Soc. London A244 (1951) 87.
3. Eshelby, J.D., "Energy Relations and the Energy-Momentum Tensor in Continuum Mechanics," Inelastic Behavior of Solids, M.F. Kanninen, et al. (eds) McGraw-Hill, New York (1970).
4. Eshelby, J.D., "The Elastic Energy-Momentum Tensor," J. Elasticity 5 (1975) 321-335.
5. Günther, Wilhelm, "Über einige Randintegrale der Elastomechanik," Abhandlungen der Braunschweigischen Wissenschaftlichen Gesellschaft Vol. XIV Verlag Friedr. Vieweg & Sohn, Braunschweig (1962).

6. Rice, J.R., "A Path-Independent Integral and the Approximate Analysis of Strain Concentrations by Notches and Cracks," J. Appl. Mech. 35 (1968) 379.
7. Knowles, J.K. and Sternberg, Eli, "On a Class of Conservation Laws in Linearized and Finite Elastostatics," Arch. Rat. Mech. Anal. 44 (1972) 187-211.
8. Budiansky, B. and Rice, J.R., "Conservation Laws and Energy-Release Rates," J. Appl. Mech. 40 (1973) 201-203.
9. Kaul, R.K., Private communication.
10. Kane, T.R., Private communication.
11. Rogula, D., "Forces in Material Space," Arch. Mech. 29 (1977) 705-713.
12. Herrmann, G., "On Variational Principles in Thermoelasticity and Heat Conduction," Q. Appl. Math. 21 (1963) 151-155.
13. Biot, M.A., "Thermoelasticity and Irreversible Thermodynamics," J. Appl. Phys. 27 (1956) 240-253.
14. Gurtin, M.E., "On a Path-Independent Integral for Elastodynamics," Int. J. Fract. Mech. 12 (1976) 643-644.
15. Sih, G.C., Handbook of Stress-Intensity Factors Vol. I, Lehigh University, Bethlehem, PA (1973).
16. Herrmann, G. and Kino, G., "Ultrasonic Measurements of Inhomogeneous Stress Fields," Proceedings of the ARPA/AFML Review of Progress in Quantitative NDE held at the Scripps Institute of Oceanography, La Jolla, CA (1978).

#### FIGURE CAPTION

Fig. 1 Integration Contour

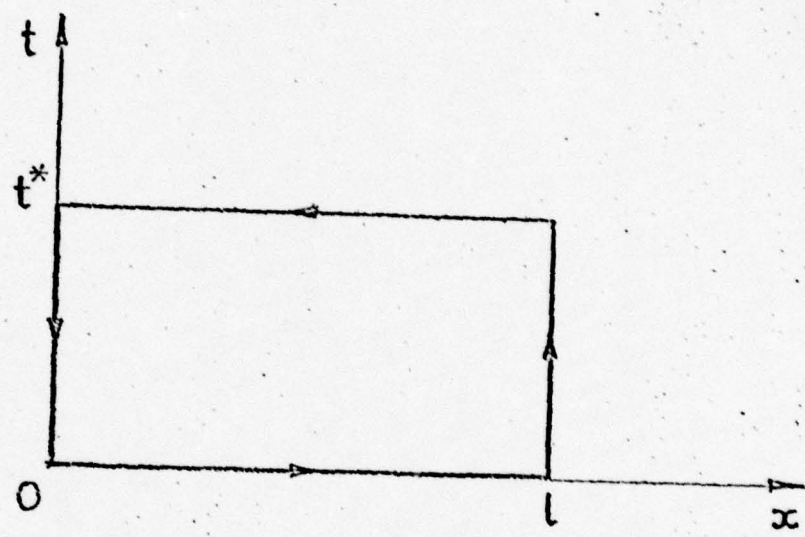


FIGURE 1

## STUDIES OF STEEL MICROSTRUCTURE BY ACOUSTICAL METHODS

N. Grayell, D. B. Ilic, F. Stanke, C. H. Chou, and J. C. Shyne

Stanford University  
Stanford, California 94305

### Abstract

We are using measurements of acoustic velocity and attenuation for nondestructive characterization of the microstructure of materials. The spatial variation of the acoustic velocity in Jominy end-quench specimens was found to correlate very well with Rockwell C hardness scans, indicating a potentially practical method for measuring the hardening response of heat treated steel. Attenuation measurements have also been performed by using broadband acoustic pulses corrected for transducer response, liquid buffer/solid specimen reflections, and diffraction effects. Higher attenuation was observed for pearlitic than for martensitic microstructures.

Mechanical properties of materials, such as tensile strength, hardness, and impact toughness, are strongly dependent on microstructural features like grain size and shape, the proportions and spatial distribution of the phases present, and macroscale heterogeneities in microstructure resulting from local compositional or thermal-mechanical processing variations. This is true of both metallic and ceramic materials. The microstructural character of materials and their related properties are usually assessed by microscopic examination or by direct measurement of properties; such procedures are often costly, and are necessarily destructive, requiring sacrificial example specimens.

Steels are alloys of iron and carbon modified by minor additions of other elements, which exhibit remarkable variability of mechanical properties. These useful properties are dependent upon the rather complex microstructure of steel which can be closely controlled by proper selection of composition and heat treatment.

The dependence of steel microstructure on composition and heat treatment is illustrated in Fig. 1. Figures 1(a) and 1(b) compare the microscopic appearance of polished and etched steel specimens containing 0.2 and 0.6 wt. pct. carbon respectively; after annealing at 900°C and slow cooling in air to room temperature both steels consist of ferrite, the white grains, and pearlite, the darker constituent. Ferrite is essentially pure

iron; pearlite is a mixture of two different crystalline phases (too finely dispersed to be resolved at the magnification shown), iron carbide ( $Fe_3C$ ) and ferrite. Since virtually all the carbon resides in the pearlite, the proportion of pearlite is greater in the higher carbon steel. Figure 1(c) shows a steel with 0.4 wt. pct. carbon with a martensitic microstructure rather than pearlite and ferrite. This steel has been cooled rapidly in water after annealing at 900°C; the fast cooling causes the formation of martensite, a supersaturated solid solution of carbon in iron. Mechanical properties are strongly affected by the proportions of ferrite and pearlite and by the existence of martensite rather than pearlite and ferrite. Changes in microstructure such as these, enable steels to be heat treated to obtain optimum combinations of properties.

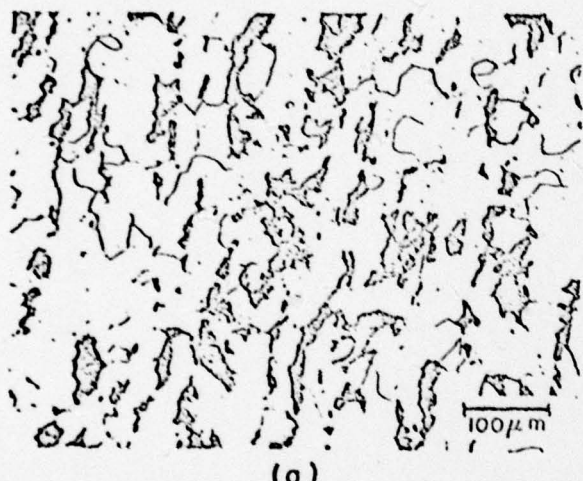
Our measurements of longitudinal acoustic wave velocity in metallic samples were made with a computer-controlled system developed for measuring acoustic velocity fields in solid samples immersed in a liquid buffer and described in detail in an accompanying paper at this conference.<sup>1</sup>

### 1. Absolute Velocity Measurements

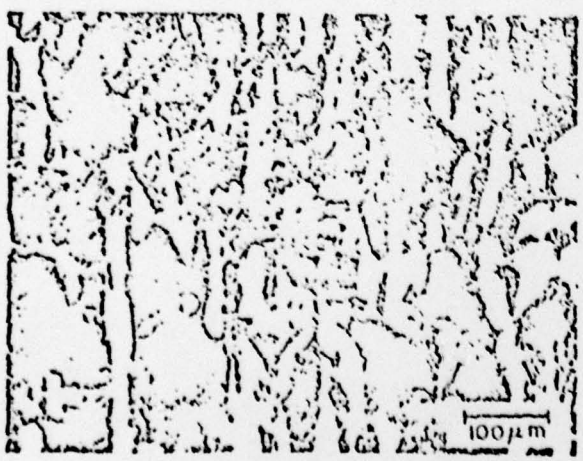
Specimens of 5 plain carbon steels were prepared by machining 1 cm thick flat plates oriented both longitudinally and transversely relative to the steel bar stock. Since the acoustic wave propagation direction was through the 1 cm plate thickness, acoustic velocity could be measured both parallel to and transverse to the rolling direction for each steel composition to detect the influence of any preferred orientation or crystal texturing. The compositions of the steels are shown in Table 1. All specimens were given identical heat treatment; they were heated to 900°C and air cooled (normalized). This resulted in pearlite/ferrite microstructures, the pearlite varying from 12 to 100 volume pct. over the range of carbon contents. After machining, the flat specimens were lapped to assure that their flat surfaces were parallel to within 2.5  $\mu m$ .

The resulting velocity measurements, which include correction for diffraction effects, exhibited random scatter that totally obscured the variation of velocity anticipated from the variation in microstructure, Fig. 2. One can

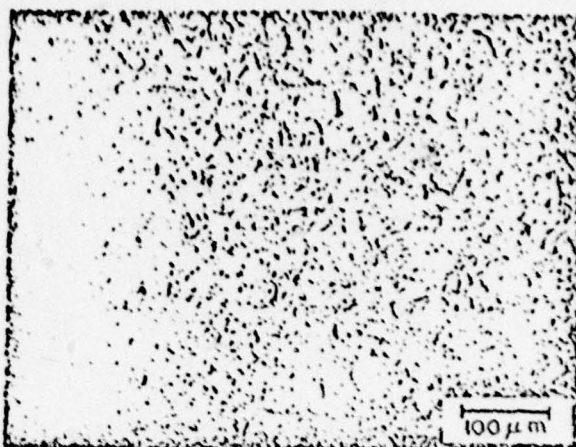
easily calculate an expected acoustic velocity from the known densities of pure iron ferrite<sup>2</sup> and Fe<sub>3</sub>C, and known elastic constant data for ferrite/Fe<sub>3</sub>C mixtures.<sup>4</sup> Increasing carbon should cause a decrease in the longitudinal acoustic velocity linearly proportional to carbon content; velocity should decrease 0.85 pct. per wt. pct. carbon in the steel, all other factors being identical. The scatter observed in the measured velocity was not caused by variations in preferred orientation; had there been any significant degree of preferred orientation, the longitudinal and transverse velocities would differ much more than the slight variations, seen in Fig. 2. We believe that the random variations in such elements as manganese, silicon, sulfur, and others always present in at least trace amounts, cause variations in density and elastic modulus and thus introduce random variations in acoustic velocity equal to or greater than the systematic effect of carbon in changing the microstructure. For example, we have calculated that the range of manganese contents in our specimens (see Table I) causes density variations large enough to obscure all the above change attributable to variations in microstructure. Therefore we conclude that absolute velocity measurements are not practical means for characterizing steel microstructure, because random compositional variations will confuse any attempt to calibrate absolute acoustic velocity variation with microstructure.



(a)



(b)



(c)

Fig. 1. Different steel microstructures resulting from difference in composition and heat treatment. (a) pearlite and ferrite in normalized 0.2 wt. pct. C steel; (b) pearlite and ferrite in normalized 0.6 wt. pct. C steel; (c) martensite in water quenched 0.4 wt. pct. C steel

TABLE I

Composition of Plain Carbon Steels used for Acoustic Velocity Measurements

Steel Type (AISI)	C	Mn	Si	P	S
1010	0.10	0.45	0.03	0.007	0.032
1020	0.20	0.52	0.21	0.009	0.028
1035	0.33	0.72	0.17	0.018	0.025
1060	0.55	0.80	0.19	0.012	0.023
1095	0.93	0.50	0.22	0.009	0.030

## MEASURED ACOUSTIC VELOCITY

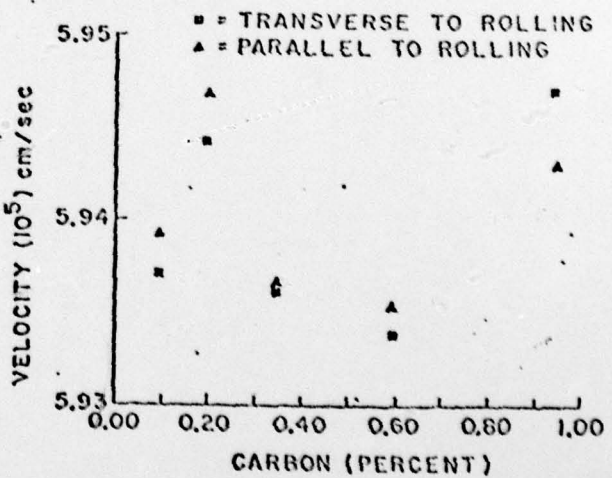


Fig. 2. Measured acoustic velocity in plain carbon steels of varying carbon content. The random scatter caused by minor fluctuations in alloying elements obscures the systematic variation in velocity related to the microstructure.

## 2. Relative Velocity Measurements

By relative velocity measurements we mean measurements of acoustic velocity at different locations within a given object. If the material composition is uniform within the object (as is usually the case), variations in acoustic velocity can be unequivocally related to microstructural variations from one location to another. There are many situations where microstructure is not uniform and the pattern of microstructural variation is important, e.g., in an induction hardened steel shaft heat treated to be martensitic on the outer surface but pearlitic in its interior. Jominy end-quench test bars provide another example of steel objects containing microstructural gradients. We successfully used relative velocity measurements to survey quantitatively the microstructure of end-quench test bars of several different alloy steel compositions.

The Jominy Test or End-Quench Test is the standard metallurgical quality control procedure for measuring the hardening response of heat treatable steels. The end-quench test specimen is a one-inch diameter round bar, four inches long. The bar is heated to about 850°C. It is then placed in a fixture and cooled by a jet of cold water impinged upon one end as shown in Fig. 3. This results in uniaxial heat flow toward the water-quenched end, and reproducible cooling rates that decrease with increasing distance away from the rapidly-cooled quenched end. The fast cooling rate at the quenched end causes the formation of hard, strong martensite; the slower cooled end transforms to softer, weaker pearlite or a pearlite and ferrite mixture, depending on composition. At intermediate locations mixed martenxite/pearlite microstructures result from the intermediate cooling rates. The position of the transition from martensite to pearlite is a measure of the hardening response. The usual way of assessing the microstructural gradient along the length of an end-quench bar is to survey the Rockwell C hardness measured on flats ground along the side of the end quench test bar. This is possible because there is a pronounced hardness gradient caused by the microstructural gradient. Although surveying hardness is a great deal easier and less time consuming than directly observing the microstructure under a microscope, the hardness surveys are tedious because up to 60 individual manual hardness measurements may be required to survey a single test bar, a procedure taking about one hour.

Figure 4 compares a conventional hardness survey with a longitudinal velocity scan of an end-quench test bar of AISI type 4140, a common, low alloy, heat-treatable steel. The longitudinal acoustic wave velocity was measured by the method described above.<sup>1</sup> The acoustic path was transverse to the axis of the test bar. Parallel flats were ground on opposite sides the full length of the test bar; the acoustic path was thus along bar diameters through the thickness of the bar between the ground flats. The relative acoustic velocity is plotted as  $\Delta v/v_0$ , the fractional change in velocity at any point relative to  $v_0$  the velocity

at the slower cooled, pearlitic end of the test bar. As seen in the plot, the velocity decreased by about 0.7 pct. at the martensitic, quenched end. The accuracy of the relative acoustic velocity measurement is limited by the uniformity of the thickness and the deviation from perfect parallelism of the ground flats. This is estimated by be 1 or 2 parts in  $10^4$  which is about 2% of the actual range of velocities measured. Thus the sensitivity and discrimination of the velocity measurement is equal to or better than that of the hardness measurements.

DIAGRAM OF A JOMINY TEST IN ACTION

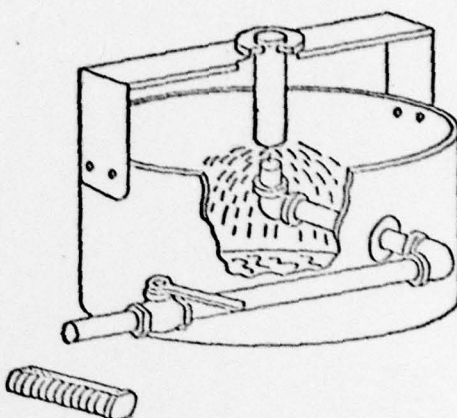


Fig. 3. End-quench test.

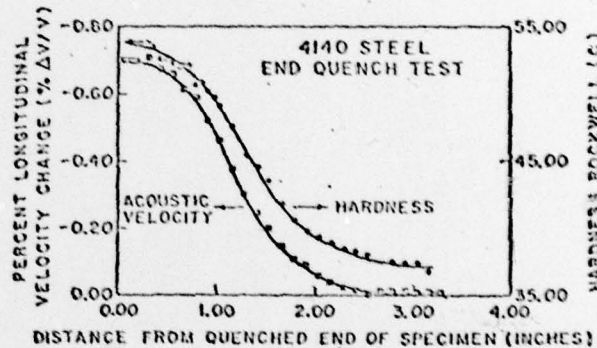


Fig. 4. End-quench test results measured in type 4140 steel. The two curves compare the microstructure gradient as surveyed acoustically and by conventional hardness measurements.

Figure 5 is a cross plot showing the relative velocity change  $\Delta v/v_0$ , versus the hardness. The correlation is virtually linear except for the extreme values. However, it is the intermediate values that are most important, because these occur at the region of transition from martensite to pearlite, the location critical to the measurement of hardening response.

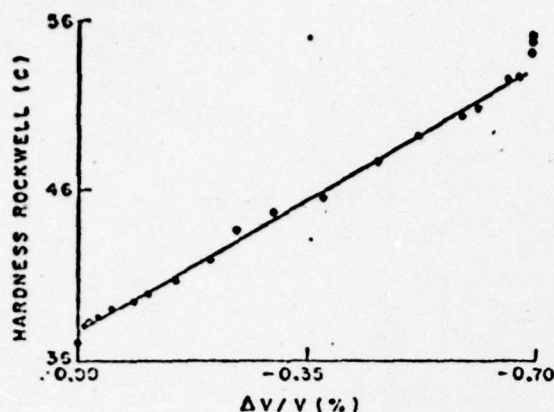


Fig. 5. Relative acoustic velocity vs. hardness Rockwell C correlated for the data shown in Fig. 4.

The computer controlled automatic acoustic velocity scan requires only 4 minutes from start to finish with the data automatically plotted as  $\Delta v/v_0$  vs. position in the bar. This contrasts favorably with the hour or so required for a manual hardness survey. To our knowledge, this is the first time an end-quench test has been performed using a velocity scan rather than a hardness scan.

In addition to the 4140 steel end-quench test we have also performed similar acoustic velocity scans on end-quench test bars of types 52100, 4615, 8640, and 1095 steels with similarly encouraging results. We find these results persuasive that acoustic velocity measurements can be used to map out microstructural variations within steel objects.

### 3. Acoustic Attenuation

In principle, attenuation measurements are more attractive than velocity measurements as the basis for acoustic NDE microstructural characterization. Where velocity is weakly a function of microstructure, acoustic attenuation is strongly affected by microstructure because of scattering at grain boundaries, second phase particles, and other microstructural features.<sup>4</sup> Moreover, the strong frequency dependence of the acoustic attenuation coefficient can provide additional information related to microstructure.

A computer interfaced system has been developed for quickly and easily measuring the attenuation of acoustic waves traveling through metal samples. The same samples used for the velocity measurements can be used for attenuation measurement. A commercial ultrasonic transducer launches longitudinal waves through a water bath at normal incidence to the sample and then receives the echoes.

The three-echo method is used to determine the attenuation, as described by Papadakis.<sup>5</sup> This method uses the measured amplitudes of three echoes to solve the equations for these echoes for any of the three unknowns in the system. In our experi-

ment, these unknowns are the pulse-echo frequency response of the system, the reflection coefficient at the sample-water interface, and the attenuation through the sample. Broadband pulses are used to obtain information over the frequency range of an octave or more. The front face echo and first two back face echoes are digitized and then stored in a computer. Since the dynamic range of these echoes can be 40 dB or more, many samples of each echo are averaged to improve the signal-to-noise ratio. The echoes are gated and separated in the computer, and the moduli of their Fourier transforms are computed by an FFT program. The spectral components of the three echoes at each frequency are compared in the three-echo method to calculate the attenuation through the sample, correcting for transducer response and also for reflection and diffraction losses. Figure 6 illustrates the importance of including the diffraction correction. The scales are logarithmic, log dB/cm versus log f, so that the slopes of the linear plots give the powers of the frequency dependence. These curves are plotted by a computer by simply connecting 128 attenuation data points within the passband. No curve fitting techniques have been used. One measurement produces a large amount of attenuation information about the sample.

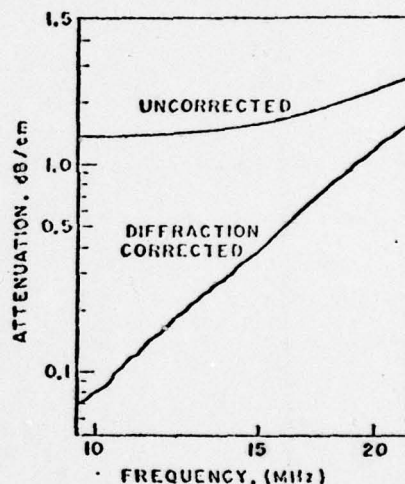


Fig. 6. Attenuation vs. frequency for a steel sample illustrating the importance of corrections for diffraction.

Figure 7 shows the attenuation in two different steel samples with identical compositions but different microstructure. The curves for pearlite and martensite show frequency dependences close to  $f^4$  indicating that Rayleigh scattering is the dominant mechanism for attenuation. Pearlitic data was obtained from two different transducers, as shown by the overlap on the figure. These results are comparable to previous results by Papadakis.<sup>6</sup>

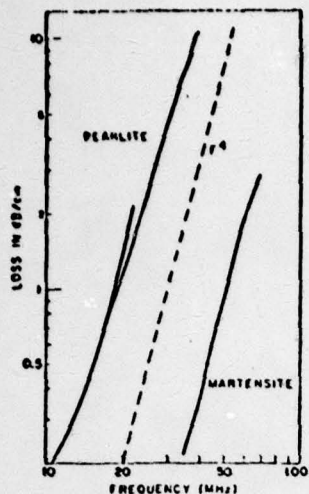


Fig. 7. Attenuation vs. frequency for two specimens of the same steel heat treated differently to have martensite in one but pearlite in the other.

#### 4. Conclusions

4.1 Absolute acoustic velocity measurements are subject to random variations that limit their utility for microstructural NDE.

4.2 Relative velocity change measurements can be used to map microstructure with precision in a given piece of steel.

4.3 Acoustic attenuation measurements are very sensitive to microstructure, and they have good potential for practical, microstructural NDE.

#### Acknowledgments

This work was sponsored by the Air Force Office of Scientific Research under Grant AF78-3726. The experimental steels were provided by the U. S. Steel Corporation.

#### References

1. D. B. Ilić, G. S. Kino, A. R. Selfridge, and F. E. Stanke, paper GG-2 of this conference.
2. G. S. Barnett and T. B. Massalski, Structure of Metals, McGraw-Hill, 1966, p. 628.
3. W. Hume-Rothery, The Structures of Alloys of Iron, Pergamon Press, 1966, p. 140.
4. L. A. Glikman, A. M. Kartashov, Z. M. Ruashkina, and A. F. Lobov, Met. Sci. Heat Treat., 17, 5-6 (May-June 1975), pp. 398-399.
5. E. P. Papadakis, K. A. Fowler, and L. C. Lynnworth, J. Acoust. Soc. Am., 53, (1973), p. 1336.
6. E. P. Papadakis, J. Appl. Phys., 35, (1964), p. 1474.

## ACOUSTIC MEASUREMENT OF MICROSTRUCTURES IN STEELS

N. Grayell, D. B. Illic, F. Stanke, G. S. Kino, and J. C. Shyne  
Stanford University  
Stanford, California 94305

### ABSTRACT

The measurement of acoustic properties can be used for the nondestructive characterization of the microstructure of materials. We have measured the changes in longitudinal acoustic wave velocity and acoustic attenuation in steel specimens whose microstructure and properties differ widely because of differing compositions and heat treatment. The spatial variation of the relative acoustic velocity in standard Jominy end-quench hardenability test specimens was found to correlate very well with Rockwell C hardness scans, indicating a potentially practical method for measuring the hardening response of heat treated steel. Absolute velocity measurements on steel specimens were found to be subject to random scatter related to minor compositional variations; this limits the utility of absolute velocity measurements for microstructural NDE. Attenuation measurements have also been performed on steel samples with different microstructures. The measurement utilized broadband acoustic pulses corrected for transducer response, liquid buffer/solid specimen reflection, and diffraction effects. Attenuation coefficients were seen to be proportional to frequency squared for martensite and to the fourth power of frequency for pearlite. Higher attenuation was observed for pearlitic than for martensitic microstructures.

Acoustic methods can be applied to the nondestructive characterization of the microstructure of materials. This paper reports the initial efforts of our interdisciplinary program to explore microstructural acoustic NDE. The experimental materials were steels.

The properties of materials, especially mechanical properties such as tensile strength, hardness, and impact toughness, are strongly dependent on microstructural features like grain size and shape, the proportions and spatial distribution of the phases present, and macroscale heterogeneities in microstructure resulting from local compositional or thermal-mechanical processing variations. This is true of both metallic and ceramic materials. The microstructural character of materials and their related properties are usually assessed by microscopic examination or by direct measurement of properties; such procedures are often costly, and are necessarily destructive, requiring sacrificial example specimens.

Steels are basically alloys of iron and carbon modified by minor additions of other elements. Steels exhibit remarkable variability of mechanical properties. These useful properties are dependent upon the rather complex microstructure of steel which can be closely controlled by proper selection of composition and heat treatment.

The dependence of steel microstructure on composition and heat treatment is illustrated in Fig. 1. Figures 1(a) and 1(b) compare the microscopic appearance of polished and etched steel specimens containing 0.2 and 0.6 wt. pct. carbon respectively; after annealing at 900°C and slow cooling in air to room temperature both steels consist of ferrite, the white grains, and pearlite, the darker constituent. Ferrite is essentially pure iron; pearlite is a mixture of two different crystalline phases (too finely dispersed to be resolved at the magnification shown), iron carbide ( $Fe_3C$ ) and ferrite. Since virtually all the carbon resides in the pearlite, the proportion of pearlite is greater in the higher carbon steel. Figure 1(c) shows a steel with 0.4 wt pct carbon with a martensitic microstructure

rather than pearlite and ferrite. This steel has been cooled rapidly in water after annealing at 900°C; the fast cooling causes the formation of martensite, a supersaturated solid solution of carbon in iron. Mechanical properties are strongly affected by the proportions of ferrite and pearlite and by the existence of martensite rather than pearlite and ferrite. Changes in microstructure such as these, enable steels to be heat treated to obtain optimum combinations of properties.

### ACOUSTIC VELOCITY MEASUREMENT

Our measurements of longitudinal acoustic wave velocity in metallic samples were made with a computer-controlled system developed for measuring acoustic velocity fields in solid samples immersed in a liquid buffer. The measurements use a two pulse-echo technique that cancels out the effects of the liquid buffer. The measuring method is illustrated in Fig. 2. Two sets of tone bursts several rf cycles long are transmitted, and their reflections from the specimen are received by a mechanically scanning commercial transducer. The delay between the two pulses is adjusted to overlap the back-face echo of the first pulse with the front-face echo of the second pulse, and this sum is gated out and detected. The product term is then used as an error signal in a phase-lock loop, which adjusts the frequency to keep the phase difference between the two echoes constant. Effectively, the measurement of phase change introduced by propagation through the specimen is converted to that of frequency, which can be performed with great precision. All of the above operations, including the mechanical scanning of the transducer, data collection, reduction, and display are controlled by a PDP 11-34 minicomputer. The resulting system precision is about 1 part in  $10^6$  of the measured longitudinal acoustic velocity. The accuracy of the absolute velocity measurement is 2 parts in  $10^4$ , as dictated by the accuracy in measuring the acoustic path length, the specimen thickness.

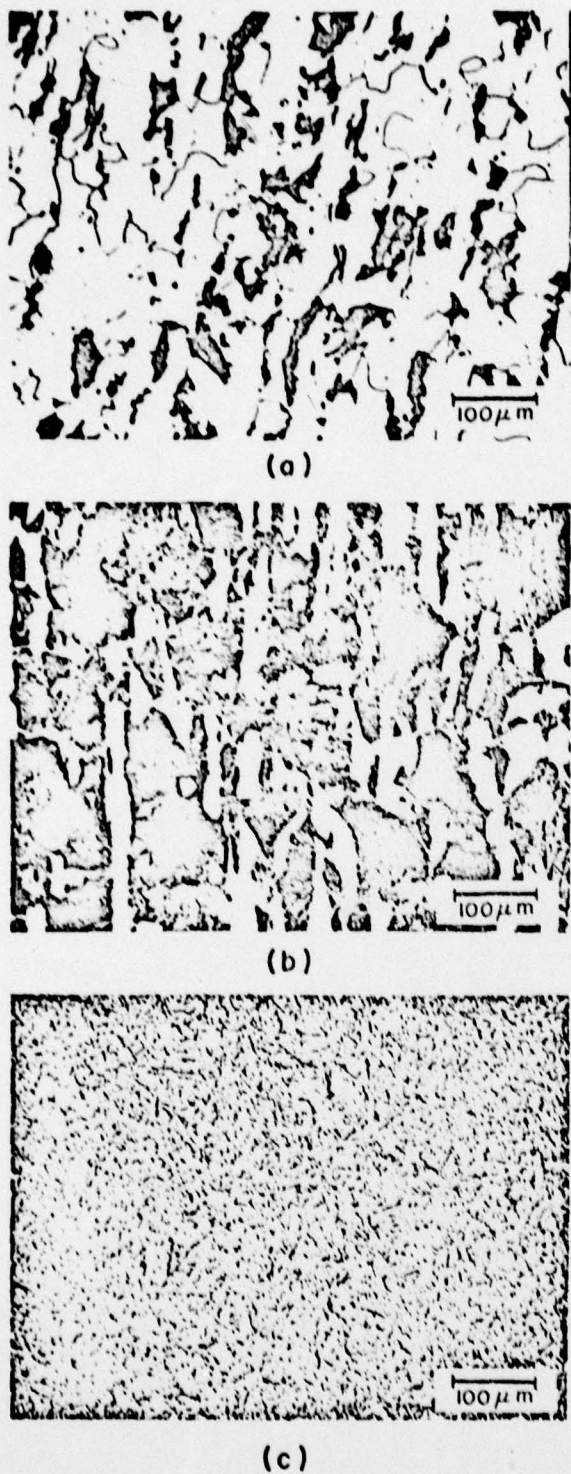


**FIG. 1.** Different steel microstructures resulting from difference in composition and heat treatment. 1(a): pearlite and ferrite in normalized 0.2 wt pct C steel; 1(b): pearlite and ferrite in normalized 0.6 wt pct C steel; 1(c): martensite in water quenched 0.4 wt pct C steel.

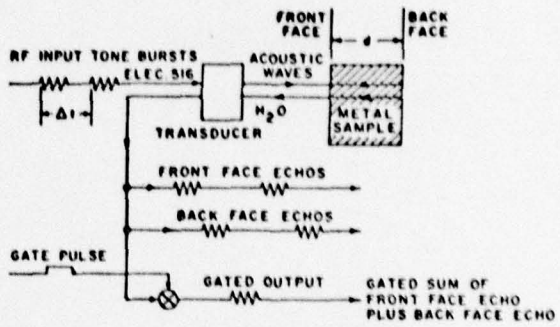


**FIG. 2.** Schematic of the precision acoustic velocity measuring system.

#### ABSOLUTE VELOCITY MEASUREMENTS

Specimens of 5 plain carbon steels were prepared by machining 1 cm thick flat plates oriented both longitudinally and transversely relative to the steel bar stock. Since the acoustic wave propagation direction was through the 1 cm plate thickness, acoustic velocity could be measured both parallel to and transverse to the rolling direction for each steel composition to detect the influence of any preferred orientation or crystal texturing. The compositions of the steels are shown in Table I. All specimens were given identical heat treatment; they were heated to 900°C and air cooled (normalized). This resulted in pearlite/ferrite microstructures, the pearlite varying from 12 to 100 volume pct over the range of carbon contents. After machining, the flat specimens were lapped to assure that their flat surfaces were parallel to within 2.5 μm.

**TABLE I**

Composition of Plain Carbon Steels used for Acoustic Velocity Measurements

Steel Type (AISI)	C	Mn	Si	P	S
1010	0.10	0.45	0.03	0.007	0.032
1020	0.20	0.52	0.21	0.009	0.028
1035	0.33	0.72	0.17	0.018	0.025
1060	0.55	0.80	0.19	0.012	0.023
1095	0.93	0.50	0.22	0.009	0.030

The resulting velocity measurements exhibited random scatter that totally obscured the variation in velocity anticipated from the variation in microstructure, Fig. 3. One can easily calculate an expected acoustic velocity from the known densities of pure iron ferrite<sup>1</sup> and Fe<sub>3</sub>C,<sup>2</sup> and known elastic constant data for ferrite/Fe<sub>3</sub>C mixtures.<sup>3</sup> Increasing carbon should cause a decrease in the longitudinal acoustic velocity linearly proportional to carbon content; velocity should decrease

0.85 pct per wt. pct carbon in the steel, all other factors being identical. The scatter observed in the measured velocity was not caused by variations in preferred orientation; had there been any significant degree of preferred orientation, the longitudinal and transverse velocities would differ much more than the slight variations, which can be attributed to sample thickness variations, seen in Fig. 3. We believe that the random variations in such elements as manganese, silicon, sulfur and others always present in at least trace amounts, cause variations in density and elastic modulus and thus introduce random variations in acoustic velocity equal to or greater than the systematic effect of carbon in changing the microstructure. For example, we have calculated that the range of manganese contents in our specimens (see Table I) causes density variations large enough to obscure all the above change attributable to variations in microstructure. Therefore we conclude that absolute velocity measurements are not practical means for characterizing steel microstructure, because random compositional variations will confuse any attempt to calibrate absolute acoustic velocity with microstructure.

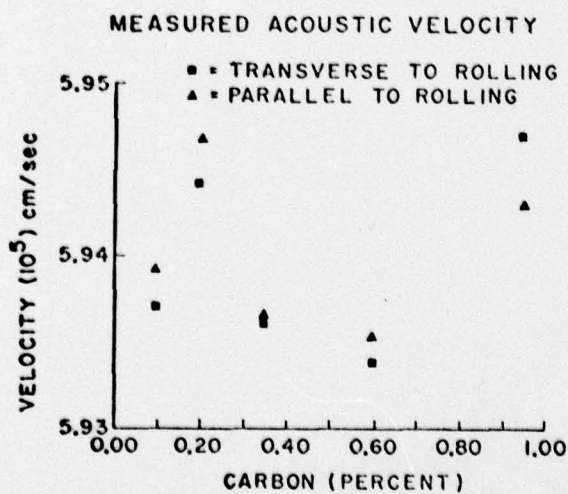


FIG. 3. Measured acoustic velocity in plain carbon steels of varying carbon content. The random scatter caused by minor fluctuations in alloying elements obscures the systematic variation in velocity related to the microstructure.

#### RELATIVE VELOCITY MEASUREMENTS

By relative velocity measurements we mean measurements of acoustic velocity at different locations within a given object. If the material composition is uniform within the object (as is usually the case), variations in acoustic velocity can be unequivocally related to microstructural variations from one location to another. There are many situations where microstructure is not uniform and the pattern of microstructural variation is important, e.g., in an induction hardened steel shaft heat treated to be martensitic on the outer surface but pearlitic in its interior. Velocity variation within a given object, i.e., relative velocity, could be

used to map out the microstructural pattern. Jominy end-quench test bars provide another example of steel objects containing microstructural gradients. We successfully used relative velocity measurements to survey quantitatively the microstructure of end quench test bars of several different alloy steel compositions.

The Jominy Test or End-Quench Test is the standard metallurgical quality control procedure for measuring the hardening response of heat treatable steels. The end-quench test specimen is a one-inch diameter round bar, four inches long. The bar is heated to about 850°C. It is then placed in a fixture and cooled by a jet of cold water impinged upon one end as shown in Fig. 4. This results in uniaxial heat flow toward the water-quenched end, and reproducible cooling rates that decrease with increasing distance away from the rapidly-cooled quenched end. The fast cooling rate at the quenched end causes the formation of hard, strong martensite; the slower cooled end transforms to softer, weaker pearlite or a pearlite and ferrite mixture, depending on composition. At intermediate locations mixed martensite/pearlite microstructures result from the intermediate cooling rates. The position of the transition from martensite to pearlite is a measure of the hardening response. The usual way of assessing the microstructural gradient along the length of an end-quench bar is to survey the Rockwell C hardness measured on flats ground along the side of the end quench test bar. This is possible because there is a pronounced hardness gradient caused by the microstructural gradient. Although surveying hardness is a great deal easier and less time consuming than directly observing the microstructure under a microscope, the hardness surveys are tedious because up to 60 individual manual hardness measurements may be required to survey a single test bar, a procedure taking about one hour.

DIAGRAM OF A JOMINY TEST IN ACTION

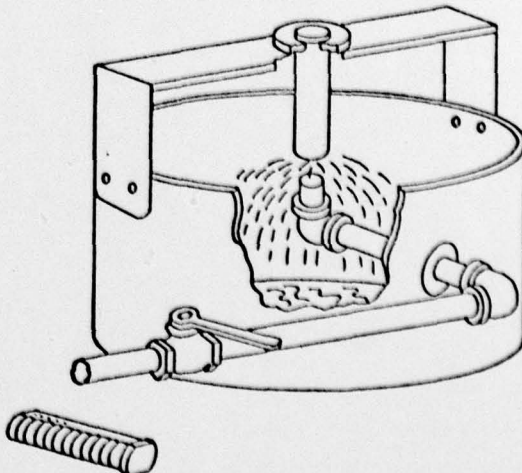


FIG. 4. End-quench test.

Figure 5 compares a conventional hardness survey with a longitudinal velocity scan of an end-quench test bar of AISI type 4140, a common, low alloy, heat-treatable steel. The longitudinal acoustic wave velocity was measured by the method described above

and illustrated in Fig. 2. The acoustic path was transverse to the axis of the test bar. Parallel flats were ground on opposite sides the full length of the test bar; the acoustic path was thus along bar diameters through the thickness of the bar between the ground flats. The relative acoustic velocity is plotted as  $\Delta V/V_0$ , the fractional change in velocity at any point relative to  $V_0$ , the velocity at the slower cooled, pearlitic end of the test bar. As seen in the plot the velocity decreased by about 0.7 pct at the martensitic, quenched end. The accuracy of the relative acoustic velocity measurement is limited by the uniformity of the thickness and the deviation from perfect parallelism of the ground flats. This is estimated to be 1 or 2 parts in  $10^4$  which is about 2% of the actual range of velocities measured. Thus the sensitivity and discrimination of the velocity measurement is equal to or better than that of the hardness measurements.

Figure 6 is a cross plot showing the relative velocity change  $\Delta V/V_0$ , versus the hardness. The correlation is virtually linear except for the extreme values. However, it is the intermediate values that are most important, because these occur at the region of transition from martensite to pearlite, the location critical to the measurement of hardening response.

The computer controlled automatic acoustic velocity scan requires only 4 minutes from start to finish with the data automatically plotted as  $\Delta V/V_0$  vs position in the bar. This contrasts favorably with the hour or so required for a manual hardness survey. To our knowledge, this is the first time an end-quench test has been performed using a velocity scan rather than a hardness scan.

In addition to the 4140 steel end-quench test we have also performed similar acoustic velocity scans on end-quench test bars of types 52100, 4615, 8640, and 1095 steels with similarly encouraging results. We find these results persuasive that acoustic velocity measurements can be used to map out microstructural variations within steel objects.

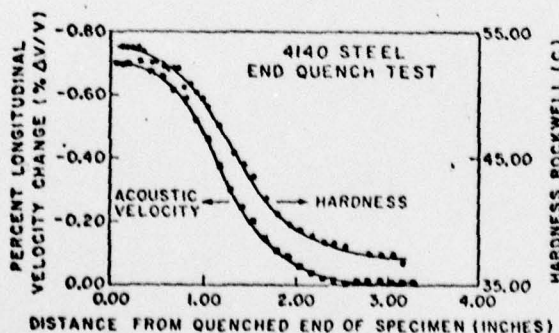


FIG. 5. End-quench test results measured in type 4140 steel. The two curves compare the microstructure gradient as surveyed acoustically and by conventional hardness measurements.

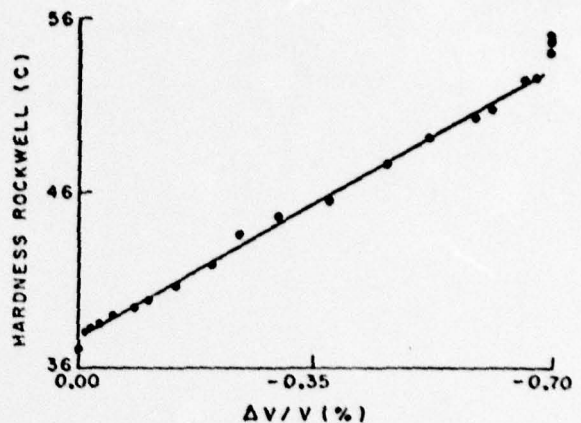


FIG. 6. Relative acoustic velocity vs hardness Rockwell C correlated for the data shown in Fig. 5.

#### ACOUSTIC ATTENUATION

In principle, attenuation measurements are more attractive than velocity measurements as the basis for acoustic NDE microstructural characterization. Where velocity is weakly a function of microstructure, acoustic attenuation is strongly affected by microstructure because of scattering at grain boundaries, second phase particles and other microstructural features.<sup>4</sup> Moreover, the strong frequency dependence of the acoustic attenuation coefficient can provide additional information related to microstructure.

This paper reports only our earliest, preliminary efforts to characterize microstructure by means of acoustic attenuation measurements.

A computer interfaced system has been developed for quickly and easily measuring the attenuation of acoustic waves traveling through metal samples. The same samples used for the velocity measurements can be used for attenuation measurement. A commercial ultrasonic transducer launches longitudinal waves through a water bath at normal incidence to the sample and then receives the echoes. Normal incidence is attained by swiveling the transducer to maximize the amplitude of the front face echo. A narrowband pulse (i.e., a tone burst with at least 10 rf cycles) must be used for this alignment because the various components of a broadband pulse are not equally affected by non-normal incidence and therefore the maximum is difficult to determine. Computer controlled digital stepping motors can also be used to move the transducer for spatial scanning.

The three-echo method is used to determine the attenuation, as described by Papadakis.<sup>4</sup> This method uses the measured amplitudes of three echoes to solve the equations for these echoes for any of the three unknowns in the system. In our experiment, these unknowns are the pulse-echo frequency response of the system, the reflection coefficient at the sample-water interface, and the attenuation through the sample. Broadband pulses are used to obtain

information over the frequency range of an octave or more. The front face echo and first two back face echoes are digitized and then stored in a computer. Since the dynamic range of these echoes can be 40 dB or more, many samples of each echo are averaged to improve the signal-to-noise ratio. The echoes are gated and separated in the computer, and the moduli of their Fourier transforms are computed by an FFT program. Figure 7 shows three gated, averaged pulses with their frequency spectra superimposed for a typical sample. The spectral components of the three echoes at each frequency are compared in the three-echo method to calculate the attenuation through the sample, correcting for transducer response and also for reflection and diffraction losses. Figure 8 illustrates the importance of including the diffraction correction for the echoes shown in Fig. 7. The scales are logarithmic, log dB/cm versus log  $f$ , so that the slopes of the linear plots give the powers of the frequency dependence. These curves are plotted by a computer and an analog plotter by simply connecting 128 attenuation data points within the passband. No curve fitting techniques have been used. One measurement produces a large amount of attenuation information about the sample.

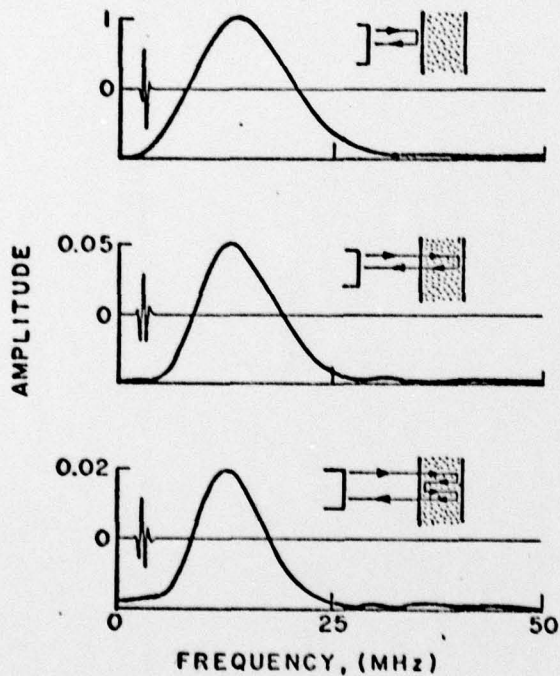


FIG. 7. Three echoes of the same broadband pulse (plotted in both the time and frequency domains) used to obtain the attenuation coefficient in the specimen for the range of frequencies in the pulse.

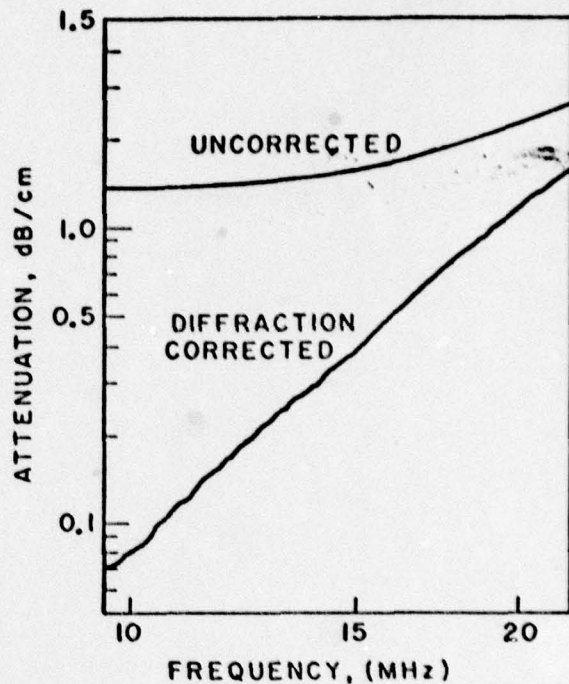


FIG. 8. Attenuation vs frequency for a steel sample illustrating the importance of corrections for diffraction.

Figure 9 shows the attenuation in two different steel samples with identical composition but

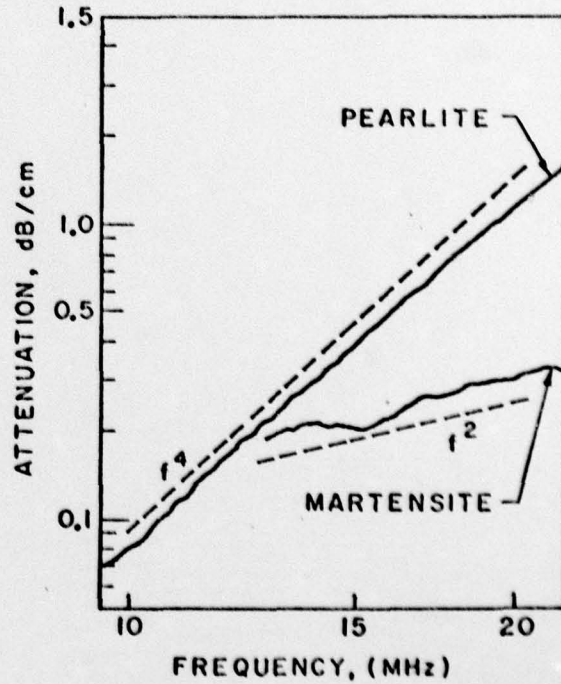


FIG. 9. Attenuation vs frequency for two specimens of the same steel heat treated differently to have martensite in one but pearlite in the other.

different microstructure. The curve for pearlite shows a frequency dependence very close to  $f^4$  indicating that Rayleigh scattering is the dominant mechanism for attenuation. The curve for martensite exhibits lower values of attenuation, with a frequency dependence nearer to  $f^2$ , indicating a different mechanism for attenuation from that in martensite. These results are comparable to previous results by Papadakis.<sup>5</sup>

#### CONCLUSIONS

1. Absolute acoustic velocity measurements are subject to random variations that limit their utility for microstructural NDE.
2. Relative velocity change measurements can be used to map microstructure with precision in a given piece of steel.
3. Acoustic attenuation measurements are very sensitive to microstructure, and they have good potential for practical, microstructural NDE.

#### ACKNOWLEDGEMENTS

This work was sponsored by the Air Force Office of Scientific Research under Grant AFOSR78-3726. The experimental steels were provided by the U.S. Steel Corporation.

#### REFERENCES

1. G. S. Barnett and T. B. Massalski, Structure of Metals, McGraw-Hill, 1966, p. 628.
2. W. Hume-Rothery, The Structures of Alloys of Iron, Pergamon Press, 1966, p. 140.
3. L. A. Glikman, A. M. Kartashov, Z. M. Ru-ashkina, and A. F. Lobov, Met. Sci. Heat Treat., 17, 5-6 (May-June 1975), pp. 398-399.
4. E. P. Papadakis, K. A. Fowler, and L. C. Lynnworth, J. Acoust. Soc. Am., 53 (1973), p. 1336.
5. E. P. Papadakis, J. Appl. Phys. 35 (1964), p. 1474.

## COMPUTER-CONTROLLED SYSTEM FOR MEASURING TWO-DIMENSIONAL ACOUSTIC VELOCITY FIELDS

D. B. III<sup>6</sup>, G. S. Kino, A. R. Selfridge, and F. E. Stanke

Ginzton Laboratory  
Stanford University  
Stanford, CA. 94305

### Abstract

An automatic system is described for measuring two-dimensional acoustic velocity fields in solid samples. The measurement is performed by a computer-controlled, mechanically-scanned transducer in a liquid bath and is based on measuring the phase delay of the acoustic wave by a two-pulse echo method. Applications include measuring stress fields due both to externally-applied and residual stresses, and microstructure studies of solid samples.

### 1. Introduction

Recently, there has been a resurgence of interest in studies of material properties by acoustic waves. Two important reasons for that development include the availability of dedicated computers for control of experiments and massive data processing, and the important expansion of the field of nondestructive materials evaluation (NDE). We report here on the development and the application to NDE of a measuring system which automatically produces two-dimensional images of stress distributions in metals and other solid materials.

The measuring technique is based on the two-pulse echo method developed some time ago,<sup>1</sup> and is applied normally to measuring propagation velocity in solid samples with bonded ultrasonic transducers.<sup>2</sup> By contrast, our experiment is carried out with a liquid buffer so that samples of a variety of shapes, sizes, and compositions can be tested by a mechanically-scanned transducer. The entire two-dimensional scanning operation is completely automated and computer-controlled, so that complete scans containing several hundred data points can be made and the results displayed in about thirty minutes. We have already reported on an early, manually-operated version of the instrument, which did not have the feature of cancelling out the water buffer propagation effects, and provided only preliminary two-dimensional scans.<sup>3</sup> A more recent publication has reported some results of acousto-elastic measurements in metals, performed on the present system.<sup>4</sup> We present here the

details of the measuring system, and then discuss some additional applications.

### 2. Measuring System

The measuring system consists of a liquid filled tank which is constructed as part of a mechanical rig for applying calibrated tensile or compressive loads to the plane-parallel specimen. As the acoustic wave velocity is changed by the applied stress, the variation of stress over the cross-section of a sample induced by external loading can be measured by a mechanically-scanned transducer while the load is being applied. The homemade, hydraulically-operated loading rig can apply loads up to  $\sim 5 \times 10^4$  N.

A piston transducer is scanned mechanically in the vertical and horizontal directions in the liquid-filled tank by a pair of computer-controlled stepping motors. The liquid employed is either water or ethylene glycol, the latter being more resistant to metal sample corrosion, the build-up of mineral deposits, and the occurrence of bubbles at the sample surface. Typically, an unfocused transducer is used to launch a beam of longitudinal acoustic waves of about 3 mm diameter at around 12 MHz.

The measurement principle is illustrated in Fig. 1. Two rf tone bursts a few  $\mu$ s long are applied to the transducer, with a variable time delay between them,  $\Delta t$ . The corresponding acoustic waves are launched such that they impinge on the sample at normal incidence, and longitudinal waves only are excited in the sample. At the liquid buffer/solid sample interface, the waves are partially transmitted and reflected; the reflected part propagates back and is received by the transducer, while the transmitted part of the acoustic energy undergoes further reflections at the sample back and front faces as it bounces back and forth inside the sample. Each one of these transits leads to some acoustic energy being transmitted back to the transducer, resulting in a corresponding received set of rf pulses. Because a liquid path is employed, the reflection coefficient, both at the front and the back of the sample, is not dependent on the bonding material and should be invariant with the transducer position.

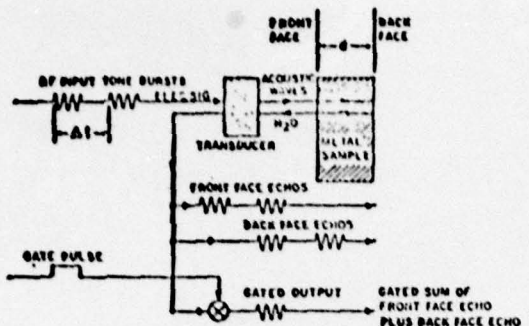


Fig. 1. The principle of the two-pulse echo measuring technique in a liquid buffer

In order to determine the local velocity of longitudinal wave propagation in the sample,  $\Delta t$  is adjusted so that the received rf pulses, due to the front-face echo of the second pulse and the back-face of the first pulse, overlap. This sum is then gated out from all the other received signals, and the phase shift between the two echoes is measured, corresponding to a double transit of the wave propagation through the sample. Thus, by using the front-face echo as the reference pulse, the wave propagation effects through the water buffer and the possible additional phase shifts in the outside circuitry are eliminated from this measurement.

### 3. Electronic Circuitry

#### 3.1 Relative Velocity

The requirement for a very precise measurement of the phase difference between the front-face and the back-face echoes, which could at the same time be automated, was met by an indirect measurement, based on a nulling technique.<sup>1</sup> Neglecting the phase shift due to the reflection at the sample back-face, the phase change which the acoustic signal undergoes in propagating through the sample of thickness  $d$  and back again to the front face is

$$\phi = \frac{4\pi f d}{v} , \quad (1)$$

where  $f$  and  $v$  are the wave frequency and velocity, respectively. For reconstructing velocity profiles in samples, we need only be concerned with velocity or transit time changes in moving from one point to the next. If we vary the carrier frequency of the rf pulses by such amounts as to keep  $\phi = \text{const}$  at every point during a scan, we obtain from Eq. (1)

$$\frac{\Delta f}{f} = \frac{\Delta v}{v} - \frac{\Delta d}{d} . \quad (2)$$

It has been shown that when stress is applied, both the relative change in velocity  $\Delta v/v$  and the relative change in thickness  $\Delta d/d$  are proportional to the applied stress.<sup>4</sup> Thus, the contours of constant stress in a sample are equivalent to contours of constant frequency for which  $\phi = \text{const}$ . It is also seen that the constant phase shifts due to reflections drop out of this relative measurement, but are needed for an absolute measurement of velocity.

The system is required to measure the phase difference between the carriers of two coincident pulses. This could be done by varying the amplitudes of the two pulses so that they tend to cancel when they are  $\pi$  out of phase, but such a technique is not conven-

tient and is highly amplitude-sensitive. We therefore adopted a sampling technique in which the basic pulse repetition rate is 8 kHz but one of the pulses has its sign reversed at a 1 kHz rate. This makes it possible to use a square law detector to obtain a 1 kHz output which depends only on the product of the two pulses of interest. This product term in turn has zero amplitude when the two rf pulses have carriers  $\pi/2$  out of phase with each other. A lock-in amplifier is employed to compare the 1 kHz detected signal with a 1 kHz reference so that the system can be made extremely sensitive. Furthermore, the output of the lock-in amplifier is itself employed to control a phase-lock loop, which changes the frequency of the input carrier so as to set the phase difference between the carriers of the two return pulses at  $\pi/2$ . Thus, the measurement system is entirely automatic.

The circuit for performing the measurement and producing results in the form of hard-copy contour plots or pictorial scan converter output is shown in Fig. 2. A free-running oscillator at 8 kHz sets the square wave pulse repetition rate and triggers the excitation of the sets of two-pulse sequences. The second pulse is further modulated by a 1 kHz signal, applied through a transistor switch (TS) in such a way that at the 8 kHz repetition rate, the square waves change sign after every four pulses. The two sets of square waves are then mixed with the output of a free-running, highly stable synthesizer (Hewlett-Packard 8660C); the resulting rf tone bursts are added, amplified by a 40 dB power amplifier and transmitted by the ultrasonic transducer.

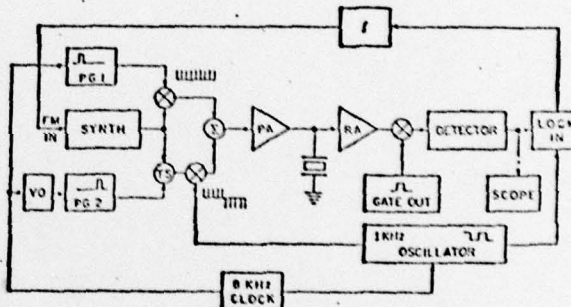


Fig. 2. Detailed block diagram of the measuring system. PG - pulse generators; VD - variable delay; PA - power amplifier; RA - limiter and receiving amplifier; SCOPE - oscilloscope monitor; LOCK-IN - lock-in amplifier; SYNTH - synthesizer of rf carrier.

The received signal from the same transducer is passed through a limiter which protects the sensitive receiver from the strong transmitted signal, and then amplified by a 60 dB variable gain receiving amplifier. That signal is displayed by the oscilloscope, at which time various adjustments and calibrations are performed. Only the desired overlap of the front and back-face echoes indicated in Fig. 1 is then gated out and detected by a balanced detector (the square law detector). The signal component at 1 kHz is then synchronously detected with a lock-in amplifier with a tuned input signal channel.

In analyzing the received and gated signals, we may take the contribution from the first rf pulse signal to be of the form

$$A(t) \cos(2\pi ft + \phi) , \quad (3)$$

where  $A(t)$  is the pulse modulation at a repetition rate of 8 kHz. Similarly, the contribution from the second pulse, which has not propagated through the sample, has the form

$$A(t)B(t) \cos 2\pi ft . \quad (4)$$

where  $B(t)$  is the 1 kHz square wave modulation of the second pulse. We note that  $B(t) = \pm 1$  and that there are eight samples (pulses) per cycle of  $B(t)$ . If we now square the sum of Eqs. (3) and (4) and take only the contribution at 1 kHz, the corresponding input to the lock-in amplifier becomes

$$A^2 B \cos \phi . \quad (5)$$

The output is then a DC signal proportional to  $R$ , where

$$R = A^2 \cos \psi \cos \phi , \quad (6)$$

where  $\psi$  is a constant phase shift between the reference and signal paths of the 1 kHz modulating signal, and  $\phi$  is the unknown desired phase shift.

The DC signal given by Eq. (6) is then used as an error signal in a phase-lock loop which varies the synthesizer output frequency in such a way that  $R = 0$  or

$$\phi = (2n + 3)\pi/2 , \quad (7)$$

since the loop locks onto every second null of  $\cos \phi$ . The lock-in amplifier output is first integrated (the lock-in amplifier integration constant is 1 ms, that of the integrator is 10 ms), and then applied to the FM input of the synthesizer, so that the resulting frequency  $f$  adjusts automatically to keep  $R = 0$  in Eq. (6). This frequency is then read into the computer via an electronic counter, and the single-point measurement is completed.

### 3.2 Absolute Velocity

For performing absolute velocity measurements, the rf carrier frequency is varied over a wide range, and several neighboring nulls corresponding to Eq. (7) are recorded. We write

$$\phi_t = \frac{4\pi f_n d}{v} + \pi - \phi_d = (2n + 3)\pi/2 , \quad (8)$$

where  $\phi_t$  is the total phase shift of the back-face echo, taking into account the  $\pi$  shift from the sample-liquid interface, and  $\phi_d$  is the contribution due to diffraction.<sup>5</sup>

An interactive computer program has been written which solves for  $v$  in two steps. First, from the slope of  $f_{n+k}$  vs.  $k$  line for several measured  $f_{n+k}$ , an approximate value of velocity  $v$  is calculated from the formula

$$v_1 = 2d(f_{n+k} - f_n)/k . \quad (9)$$

This is not accurate enough for the final calculations because it requires taking the difference of two large quantities.

The value  $v_1$  is then used for generating the diffraction phase correction, calculated numerically for our acoustic beam diameter, sample thickness, and transducer-sample distance. Eq. (8) is next solved for  $n$  using  $v = v_1$ ; since  $v_1$  is used in all

these calculations instead of the unknown  $v$ , a value very close to but not exactly equal to an integer is obtained for  $n$ . That number is then rounded off to its integer value, and  $v$  is calculated from Eq. (8). An iterative scheme of several steps could also be set up, but this first iteration gives us good accuracy.

### 3.3 Diffraction Correction

The phase change term due to diffraction  $\phi_d$  in Eq. (8), was derived in an approximate form, valid in the paraxial limit. The expression is very suitable for computer calculation, and the reader is referred for the derivation steps leading to it to a forthcoming publication.<sup>6</sup>

We are interested in the detected pressure across the face of a receiver of radius  $a$  at distance  $z$  away. The required expression is

$$\frac{\langle p_z \rangle}{\langle p_0 \rangle} = 2 \int_0^\infty e^{-j\beta z} \frac{J_1^2(\alpha a)}{\alpha} da . \quad (10)$$

Now we introduce the approximation,  $k^2 \gg a^2$ ,

$$\beta z = z\sqrt{k^2 - a^2} = kz - \frac{a^2}{2k} z , \quad (11)$$

and substituting  $S = \lambda z/a^2$ , where  $\lambda = 2\pi/k$ ,  $y = \alpha a$ , Eq. (10) becomes

$$\frac{\langle p_z \rangle}{\langle p_0 \rangle} = 2e^{-jkz} \int_0^\infty \frac{J_1^2(y)}{y} e^{jy^2 S/4\pi} dy . \quad (12)$$

This is the final expression used in computing the phase correction due to diffraction, i.e., we take

$$\phi_d = \arg \left\{ 2 \int_0^\infty \frac{J_1^2(y)}{y} e^{jy^2 S/4\pi} dy \right\} . \quad (13)$$

This expression can be evaluated very easily on the computer, and that is what we do in performing the absolute velocity measurements. As an illustration, the results of calculating Eq. (13) are plotted in Fig. 3, both for the phase and the attenuation corrections (the latter is important for correcting attenuation measurements). These results agree well with the more elaborate calculations reported in the literature.<sup>5,7</sup>

### 4. Measuring Procedure and Computer Interfacing

Initial calibration consists of mechanically aligning the transducer with respect to the sample for maximum front-face reflection, and then adjusting separately the pulse widths of PG1 and PG2 (refer to Fig. 2) such that echoes from one pulse do not overlap, depending on sample thickness and velocity of propagation. For typical samples of 1 cm thick aluminum or steel, the required pulse widths range from 1 to several  $\mu s$ . Next, the delay of the second pulse (VD) is adjusted for total overlap of the front-face echo of the second pulse with the back-face echo of the first pulse (a few  $\mu s$ ), and the attenuation (VA) adjusted for the two pulses to have about equal amplitudes. Finally, the delay of the gating signal and the appropriate pulse width of are adjusted to pick out the desired sum, and the center frequency and the FM level of the synthesizer are adjusted for appropriate excursions for proper frequency null

tracking. Typically, for the above stated conditions, the FM level is  $\sim -50$  kHz, where  $\Delta f \sim 300$  kHz corresponds to  $\Delta\theta = 2\pi$  at  $f \sim 12$  MHz. The measurement precision routinely corresponds to  $\Delta v/v$  of about  $10^{-6}$  with metal samples of the order of 1 cm thick. This is about the same or better than that obtained in the non-scanned, bonded transducer experiments based on pulse superposition, or sing-around methods.<sup>2</sup>

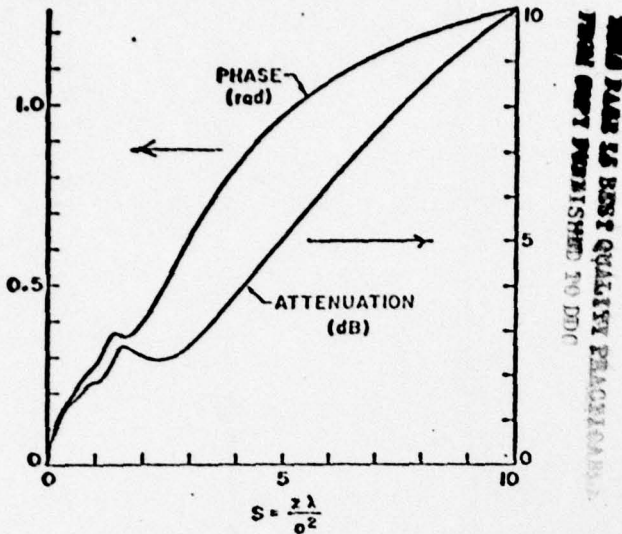


Fig. 3. Computed diffraction corrections to phase and amplitude

The measuring procedure for scanning a sample involves defining the grid of transducer positions in computer software, and after the initial sample and transducer alignment and electronics calibration, a corresponding array of frequency values of nulls of Eq. (6) is generated under complete computer control, at the rate of a few seconds per point. The data points are displayed either as contour plots of equal velocities or as equivalent scan converter output.<sup>4</sup>

### 5. Applications

The system we have described is routinely used by a varied group of electrical and mechanical engineers and materials scientists. We have already reported some exciting measurements of third order elastic constants and comparisons between measured and calculated stress fields in externally-loaded samples of different shapes.<sup>4</sup> Such contour plots can also give us very useful qualitative information about stresses around cracks and can be used to evaluate crack stress intensity factors. More recent work has included similar measurements of residual stress fields in samples with stresses built into them by a process of hydrostatic extrusion. Absolute values of radial and hoop stresses can then be obtained by suitable integration of contour data. We are just at the beginning of these latter, quantitative applications, and the prospects for NDE are exciting indeed.

We present here a recent example of the application of this system to the study of a standard end-quench Jominy bar, which is a steel rod with a widely varying hardness along its axis. The rod is normally used as a standard for measuring the hardening response to heat treatment of steel samples. It is prepared by introducing a temperature gradient along the bar axis, so that the resultant gradient in cooling rate causes a marked gradation in steel microstructure and consequently hardness. Fig. 4 shows the results of hardness (Rockwell C) measurements together with a one-

dimensional acoustic velocity scan, showing strong correlation between the two curves. It is seen that the velocity of propagation decreases as hardness is increased.

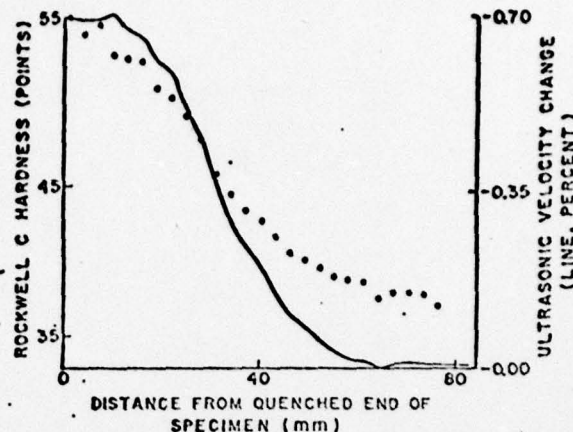


Fig. 4. Spatial dependences of Rockwell C hardness (points) and ultrasonic velocity (line) of an end-quench Jominy bar of AISI 4140 steel.  
 $v = 5.9$  km/s

Absolute velocity measurements are also being carried out with this system, as described in the previous section. This method is not as accurate as the relative measurement described, because measurements over a wide range of frequencies must be made, and extraneous factors such as diffraction corrections, amounting to about 0.15% in our case, should be taken into account.<sup>2</sup> We are also limited by the thickness accuracy of our samples to about 2  $\mu\text{m}$  on 1 cm samples, which limits the ultimate total accuracy to about  $2 \times 10^{-4}$ . This is consistent with the general statement that the precision of relative velocity scans is about two orders of magnitude better than the accuracy of absolute velocity measurements.<sup>2</sup> However, if thickness could be measured accurately, the precision of the absolute velocity measurement would be improved accordingly.

Finally, we are now preparing a shear wave scanner with specially constructed contact transducers to be used in conjunction with this system. Shear wave data will enable us to get the values of both principal stresses individually, by rotating the transducer with respect to the axis of preferred orientation, instead of just the sum of the principal stresses produced by the above longitudinal wave data.<sup>4</sup>

This work was supported by EPRI under Contract RP 609-1, NSF Contract DMK-76-00726 through the Center for Materials Research at Stanford University, and by Air Force Office of Scientific Research Grant 78-3726.

### References

1. H. J. McSkimin, *J. Acous. Soc. Am.*, **37**, 864 (1965).
2. E. P. Papadakis in *Physical Acoustics: Principles and Methods*, W. P. Mason and R. N. Thurston, eds., vol. XII, pp. 277-323 (1976).
3. J. Souquet and G. S. Kino, *J. Appl. Phys.*, **47**, 5482 (1976).
4. G. S. Kino, J. B. Hunter, G. C. Johnson, A. R. Selfridge, D. M. Barnett, G. Herrmann, and C. R. Steele, *J. Appl. Phys.*, **50**, 2607 (1979).
5. E. P. Papadakis in *Physical Acoustics: Principles and Methods*, W. P. Mason and R. N. Thurston, eds., vol. XI, pp. 151-211 (1975).
6. D. B. Ilic, G. S. Kino, and A. R. Selfridge, *Rev. Sci. Instrum.* (in press).
7. G. C. Benson and O. Kiyohara, *J. Acous. Soc. Am.*, **55**, 184 (1974).